UNIVERSITY of NEW HAMPSHIRE

Wave Energy Conservation

Mechanical Engineering Department
April 23, 2010

Aaron Williams
Megan Kramer

Advisor: Christopher White
Contributor: James Wright

Acknowledgements

This project would not have been possible without the help and support of many different individuals from both inside and outside University of New Hampshire. We would like to thank the Ocean Engineering Department at UNH and the National Sea Grant for their generous donations.This work is the result of research sponsored in part, by the National Sea Grant College Program, NOAA, Department of Commerce, under grant #NA06OAR4170109 through the New Hampshire Sea Grant College Program. We would also like to say a special thank you to those who helped make this project come to life: Sheldon Parent and James Wright who helped design and test the WEC system model, and Jennifer Bedsole who helped with ordering and finances.

Abstract

Wave energy is an attractive renewable resource due to its high energy density, but it is far less commercially developed compared to wind and solar energy. The objective of this project is to analyze the efficiency of a hydraulic power take off system in a point absorber WEC device. The conceptual idea is that a wave energy device could be used to supply supplemental energy to power a 20 ton feeder buoy, at the UNH aquaculture site, to offset the use of diesel fuel.

The WEC buoy utilizes a point absorber design. In this case there are two buoys, a large follower buoy that ideally moves on the wave surface and a long thin spar buoy that will ideally remain stationary in the center of the follower buoy. Since, the follower buoy and the spar buoy are attached, the fluid drag, or the resistance to motion caused by loads on mooring, would prevent the system from rolling and cap sizing. There are two major components that make up the interior design; the hydraulic system and the cage that holds the hydraulic system. The system begins with an forcing input from the relative displacement of the two buoy system, which drives a hydraulic piston which forces fluid though flexible hydraulic lines into an accumulator tank. The accumulator tank is an inverted two gallon aluminum tank with an air gap on the top of the tank. After the generator the fluid moves into the reservoir tank, this tank is identical to the accumulator tank except it is not inverted. The working fluid used in this system is vegetable oil.

To model all the components of the system accurately testing was conducted to determine the necessary constants of the system. This involved multiple sets of testing on the total WEC system and all of it's individually components. The efficiency over time plot shows, the sinusoidal wave approached a steady state efficiency of approximately 0.75% while the sea-state wave efficiency oscillated around 2%. The maximum efficiency for a wave capture device is 50%, and since this is a passive system the maximum expected efficiency dropped even lower to approximately 5%. Based on data obtained, plot of efficiency as a function of shaft speed, the size, rated power output of 1/2 horse power was limiting the tested system performance. The generator being used currently has too large of a frictional torque value which in turn is causing the slow angular speed. If a motor with a lower frictional torque was used in the system that the output and the efficiency would increase.

Table of Contents

List of Figures:

List of Tables

1.0 Introduction

The Department of Energy's 2008 Annual Review reports that about 80% of the world's energy supply comes from non-renewable sources such as oil, gas, and coal, while less than 20% comes from hydro, nuclear, renewable combustibles, and waste energy, and less than 1% comes from geothermal, solar, wind, and wave energy. However, with increasing global energy usage and diminishing fossil fuel supplies, there is a need for more renewable sources of energy. Wave energy is an attractive renewable resource due to its high energy density. Wave energy can produce two to three kilowatts per square meter, while wind energy produces roughly five hundred watts of power per square meter.

Although, from power density considerations, wave energy is an attractive renewable energy resource, it is far less commercially developed compared to wind and solar energy. The primary reasons for the lack of commercial development of wave energy can be contributed to both technical and economical problems related to deployment, survivability and transporting the energy generated to the necessary location. Although wave energy, at its current developmental stage, is not suited to serve as a commercial large-scale energy producing resource, it is well-suited for niche applications such as for offshore platforms and remote islands.

One suitable niche application suitable for wave energy usage is the University of New Hampshire's offshore aquaculture site which currently uses a diesel generator to produce power for a 20-ton feeder buoy. The conceptual idea is that a wave energy device could be used to supply supplemental energy to power the feeder buoy to offset the use of diesel fuel. Since the significant wave height in the northeast is approximately two meters, the available energy per unit area is approximately 39KJ/m^2. Assuming that a wave energy device with a passive control can extract approximately five percent of the total available energy, the energy available for supplemental power is approximately 2kJ/m^2. Once absorbed, the conceptual idea for energy conversion at the aquaculture site is to convert the absorbed wave energy into hydrogen, through electrolysis, and use the hydrogen as a supplemental fuel in the diesel generator. In addition to offsetting the amount of diesel fuel required to power the generator, supplementing some diesel with hydrogen has the added benefit of reducing emissions. For example, if ten percent, by energy, of the diesel fuel was replaced with hydrogen, there would be about a fifty percent reduction in controlled emissions (NOx, soot, CO) and about a five percent increase in efficiency. This is only one possible implementation of a wave energy system.

Related to the deployment of a wave energy conversion (WEC) device at the UNH aquaculture site, the objective of this project is to analyze the efficiency of a hydraulic power take off system in a point absorber WEC device. With only two group members, the original

proposal to build, deploy, and test a 1:5 scale WEC was not possible, instead the objective was to complete a full scale design, model the system components, and predict the performance of the WEC in actual sea-state conditions.

2.0 Background

2.1 Location

The WEC was designed to be deployed at the University of New Hampshire's offshore aquaculture site, located roughly ten kilometers off the coast of Portsmouth, New Hampshire and 1.8 kilometers south of the Isles of Sholes. At this location, the significant wave heights are approximately two meters. An additional benefit of the site is that it is isolated from high traffic areas so its performance will not be affected by boat generated waves and there are existing environmental buoys that monitor the sea states and other critical variables needed to assess the performance of the WEC. Based on the deployment location and an assumed capture efficiency for the WEC of 5% this yields an available energy per unit area of 2kJ/m^2. The assumed capture efficiency of 5% is typical of passive control WEC devices.

2.2 Airy Wave Theory

Airy wave theory is a mathematical model of the effects that gravity has on linearized, inviscid, incompressible, irrotational surface waves. Wave theory gives the equation for a wave's velocity potential as

$$\phi = \frac{gH}{2\sigma}\frac{\sinh\left(k(d+y)\right)}{\cosh\left(kd\right)}, \tag{1}$$

Where Φ is the velocity potential, g is gravity, H is wave height, σ is angular frequency (σ=2π/wave period), k is the wave number (2π/wavelength), and d is water depth. For deep water waves, like the ocean waves that the WEC will operate in, the wavelength to depth ratio is one half which allows the Airy wave theory to be simplified as,

$$c = \frac{gL}{2\pi}, \tag{2}$$

$$c_g = \frac{d\omega}{dk}, \tag{3}$$

These equations are used to characterize the velocity of group waves. A group wave is created when there is interference between two sinusoidal waves with different phase speed. In Equations 2 and 3 c is the wave speed, and L is the wavelength; ω is the angular velocity for the group speed, c_g. The group speed is the speed at which the waves travel as a whole, and the wave speed is the speed that an individual wave, within the group wave, travels, this can be seen in Figure 1.

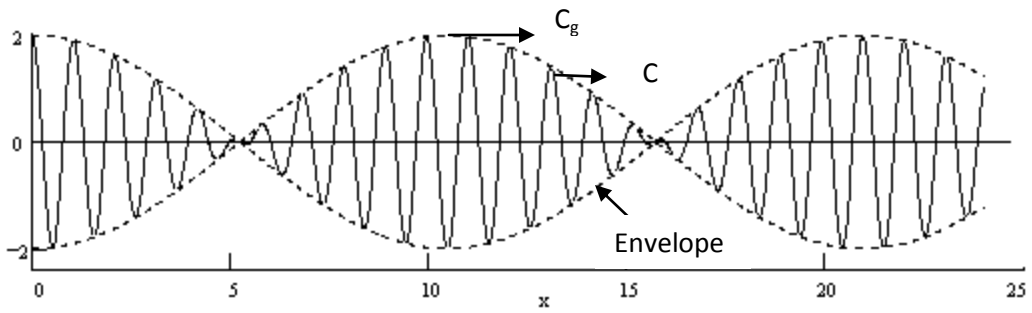

Figure 1: Shows a group wave, where c_g is the group speed and c is the wave speed. For actual group waves the envelope does not exist.

For non-dispersive waves the group speed is equal to the wave speed. This means that if there is a fixed wave length for a deep water wave, than the wave speed is not depth dependent. From the airy wave theory the equation for energy within a wave is

$$\frac{E}{A} = \frac{1}{8}\rho g H^2, \tag{4}$$

Where E/A is the energy per area and ρ is the density of the fluid medium. To find a prediction of energy in the ocean at a random sea state a significant wave height is used for the value of H, this is calculated using Equation (5).

$$H_{\frac{1}{3}} = \frac{6\sqrt{2}}{\pi}\sqrt{\frac{1}{N}\sum_{i=1}^{N} H_i^2 \sin\frac{\pi}{6}}, \tag{5}$$

Where N is the total number of waves, and H_i is the individual wave height. Since the energy per unit time is being used as a prediction and because there is limited resources for data, the significant wave height will not be calculated. Instead the generally accepted value of two meters for the north eastern American coast will be used.

2.3 Bretschneider Spectrum

The Bretschneider Spectrum is used to accurately describe the fully developed sea states found on the coast of the northeast. The Brentschneider Spectrum can be calculated using Equation 6,

$$S(\omega) = \frac{1.25}{4}\frac{\omega_m^4}{\omega^5} H_{1/3}^2 e^{-1.25(\frac{\omega_m}{\omega})^4}, \tag{6}$$

Where ω_m is the modal frequency, S is the spectral density and $H_{1/3}$ is the significant wave height found in Equation 5. The spectral density is the frequency distribution of the time average of the mean squared wave amplitude. Using Equation 6, a model of a random sea state wave can be generated, Figure 2 shows the significant wave height as a function of frequency and the surface wave amplitude over time as found by the Bretschneider Spectrum.

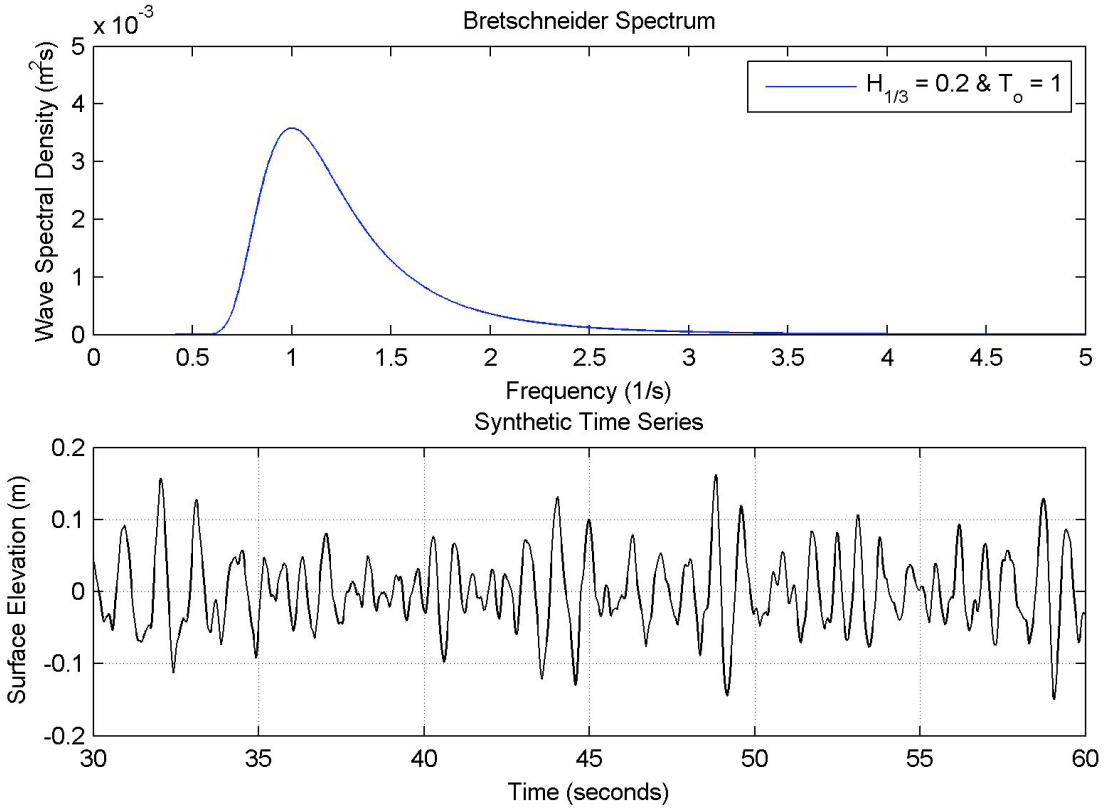

Figure 2: Using the Bretschneider Wave Spectrum a random sea state for the northeast was generated, this plot comes directly for James Wright's Thesis.

2.4 Hydraulic System

Four different elements make up the hydraulic power take-off system: (1) the piston, (2) the accumulator tank, (3) the reservoir tank, and (4) the generator. A schematic of the hydraulic power take-off system is shown in Figure 1. The arrow identifies the flow direction though the connecting hydraulic lines and each block represents a different element in the system.

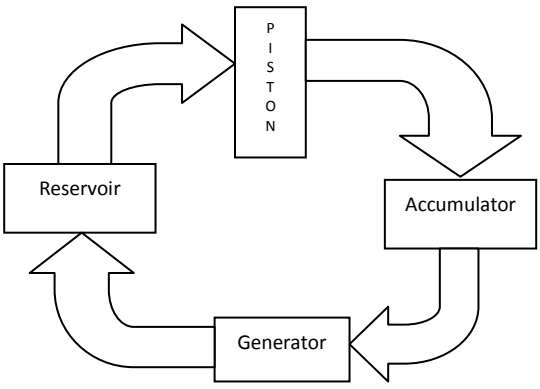

Figure 3: Conceptual model of hydraulic power take-off system.

To reduce the WEC device's environmental impact, vegetable oil will be used as the working fluid instead of standard hydraulic fluid. There disadvantages of using vegetable oil compared to standard hydraulic fluid is that vegetable oil ,unlike standard hydraulic fluid, does not have: anti-ware and anticorrosion additives, and is not fire resistance. A lack of these characteristics, however, is not necessarily a problem for this project; since when deployed the buoy will be in the Atlantic Ocean surround by cold water, which significantly reduces the chances and collateral damage of a fire in the hydraulic system. Deployment will also only be for a short, likely monitored, amount of time, a few hours or day at most, so wearing and corrosion are not a large concern.

2.5 First and Second Order Systems

By modeling each component of the WEC separately allowed a Matlab/Simulink model predicting output and efficiency of the system to be generated. The hydraulic system can be modeled as a first order system where the pressure in the system can be written similar to the way an equation would be written for an electrical system.

$$P = \int \frac{1}{C} q dt + Rq, \tag{7}$$

Where P is the pressure in the system, C is the capacitance of the system, R is the resistance to flow within the system and q is the flow rate of the system. It was assumed that there was no inductance within the hydraulic lines and the only component with capacitance was the accumulator tank.

The mechanical portion of the WEC systems generator can be written as a standard second order equation for a motor, using summation of moments for a dynamic system,

$$J\dot{\omega} = T_i - T_f - B\omega, \tag{8}$$

Where J is the moment of inertia, $\dot{\omega}$ is the angular acceleration, T_i is the input torque, T_f is the friction torque, b is the damping coefficient, and ω is the angular velocity. By relating the input torque to the flow rate Equation 8 can be rewritten as,

$$J\dot{\omega} = qk_p - T_f - B\omega, \tag{9}$$

where k_p is the pump constant. Using Kirchhoff's Voltage Law an equation modeling the electrical portion of the WEC system generator can be derived.

$$e_o = e_b - L\frac{di}{dt} - Ri, \tag{10}$$

Where e_o is the output voltage, e_b is the feedback voltage, L is the inductance of the circuit, i is the current, and R is the resistance. Relating the feedback voltage to the angular velocity of the generator, Equation 10 can be rewritten as

$$e_o = k_t \omega - L\frac{di}{dt} - Ri, \tag{11}$$

where k_t is the generator constant. By combining all of the individual systems together the total model for the WEC becomes a fifth order system. This system was then modeled using the computational software Matlab Simulink.

3.0 Design

3.1 Exterior Design

The WEC buoy utilizes a point absorber design. In this case there are two buoys, a large follower buoy that ideally moves on the wave surface and a long thin spar buoy that will ideally remain stationary in the center of the follower buoy. Figure 4 show a three dimensional representation of how the buoys will be positioned.

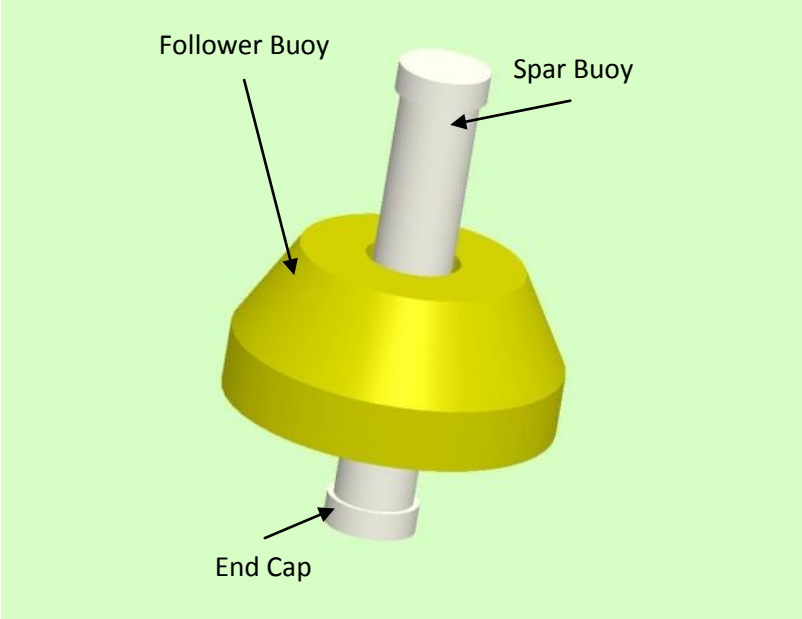

Figure 4: ProEngineered 3-D model of the spar and follower buoy.

The center spar buoy is designed to be ten feet long and twenty inches in diameter. One end cap is permanently attached to the bottom of the spar buoy and sealed while the top of the spar buoy is capped with a removable plug. This design keeps the hydraulic power take-off system within the spar buoy relatively dry while still allowing for the removal of the internal components. A three inch hole will be drilled though the plug, this will allow the piston to be coupled to the follower buoy through the outer frame, shown in Figure 5.

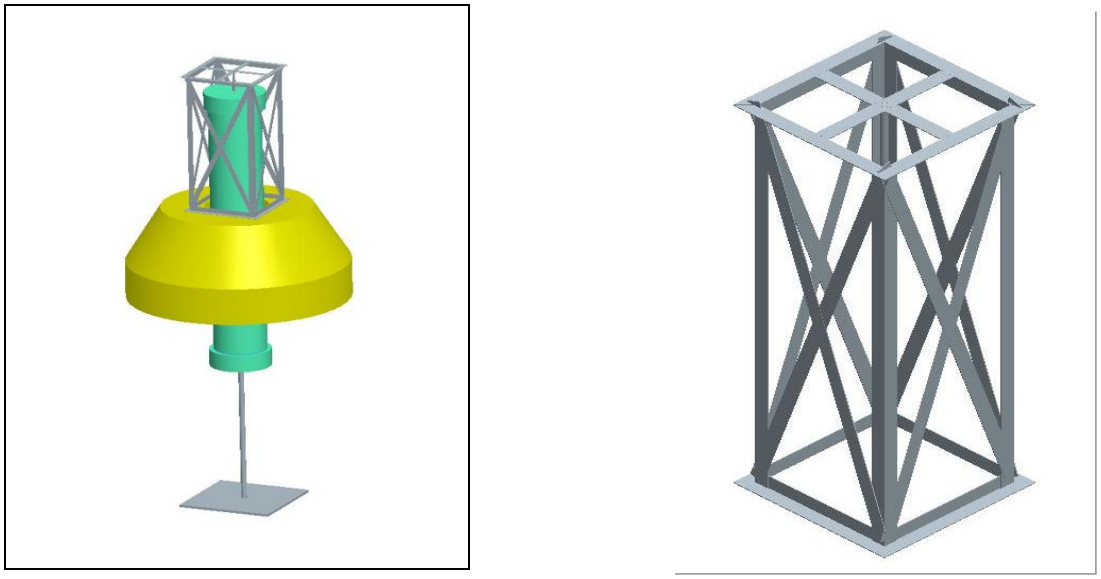

Figure 5: The left picture is a completed exterior design of the wave energy buoy (with exception of the drag plate). The picture on the right is an individual picture of the cage design.

The flat side of the follower buoy was chosen to face down so that the buoy would have a larger surface area in contact with the wave to heave more with the wave motion. Since the follower buoy is placed flat side down, there may be concerns about stability of the total system while deployed in sea waves. Since, the follower buoy and the spar buoy are attached, the fluid drag, or the resistance to motion caused by loads on mooring, would prevent the system from rolling and cap sizing.

The external cage, seen in Figure 5, will be made of low carbon steel angle irons and strips, and then coated with a corrosive resistant marine finish. Steel was chosen due to the high strength of the material as well as its low cost compared to other metals. Figure 6 shows a stress analysis of the exterior cage with a 200 lb/in^2 load applied at the center of the cage. Analysis to find the displacement due to the load and the von Mises stress were done in ProEngineer Mechanica. It was assumed that the mounting between the cage and the follower buoy were fixed points, with zero displacement. Environmental effects as well as fatigue effects were neglected due to the fact that the WEC will be deploy for short, likely supervised periods of time and would not be a permanent installation.

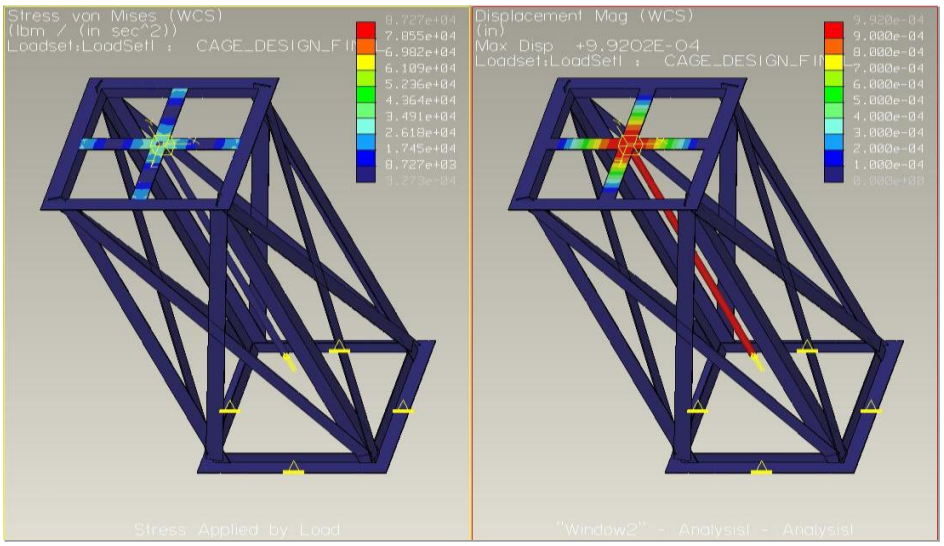

Figure 6: Stress analysis done in ProEngineer Mechanica with a 200 lb/in^2 load on the center of the structure, the picture on the left shows the magnitude of the stress von Mises in lbm/(s*in^2). The picture on the right shows the displacement caused by the load in inches.

As seen in Figure 6, neither the displacement, with a maximum of 9.0e-4 inches, nor the von Mises stress, with a maximum of 2.6e4 lbm/(s*in^2) are enough to cause failure to the cage. The 200lb/in^2 force was chosen, since it is approximately twice the expected maximum coupling force.

3.2 Interior Design

There are two major components that make up the interior design; the hydraulic system and the cage that holds the hydraulic system. There are four different elements that make up the hydraulic system: (1) the piston, (2) the accumulator tank, (3) the reservoir tank, and (4) the generator, a visual schematic can be seen in Figure 7.

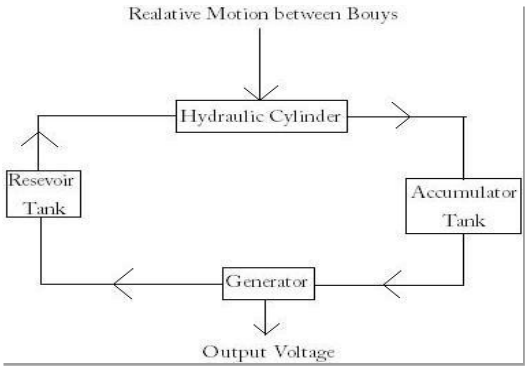

Figure 7: Visual representation of hydraulic system, show intake flow and output voltage.

The system begins with an forcing input from the relative displacement of the two buoy system, which drives a one-meter hydraulic piston which forces fluid though flexible hydraulic lines into an accumulator tank. The accumulator tank is an inverted two gallon aluminum tank with an air gap on the top of the tank. This was chosen during last year's design, which the size based on the one-gallon stroke displacement and a six second period, also because the tank is rated for carbon dioxide, this means it can withstand high pressures, ensuring that there are no leaks in the system. The accumulator tank must be inverted so that the air is on the top of the tank and can be compressed and store energy, it is also inverted to prevent any air from bleeding into the lines and seizing the pump.

Figure 8: Hydraulic system set-up for testing done on the accumulator. This photo was provided by the 2008-2009 Wave Energy Conservation group.

Next is the generator, which for this case is a half horse DC motor run in reverse. The generator is capable of a 300 watt output under ideal conditions. After the generator the fluid moves into the reservoir tank, this tank is identical to the accumulator tank except it is not inverted. Finally the fluid returns to the piston. In between each element of the system is a hydraulic line that connects to each element using copper fittings. The working fluid used in this system is vegetable oil. There are some advantages for using hydraulic fluid as a working fluid as opposed to other fluids; for example hydraulic fluid has antiwar characteristics, corrosion control, minimizes internal leakage, and is fire resistance. Most of these characteristics are not necessary for this project, for example when deployed the buoy will be in the Atlantic Ocean surround by cold water, this will significantly reduce the chances of a fire in the hydraulic system. Deployment will also only be for a short amount of time, a few hours or days at most, so wearing and corrosion are not a big concern. Vegetable oil was chosen for two reasons; it is low in cost, and more environmentally friendly than alternatives.

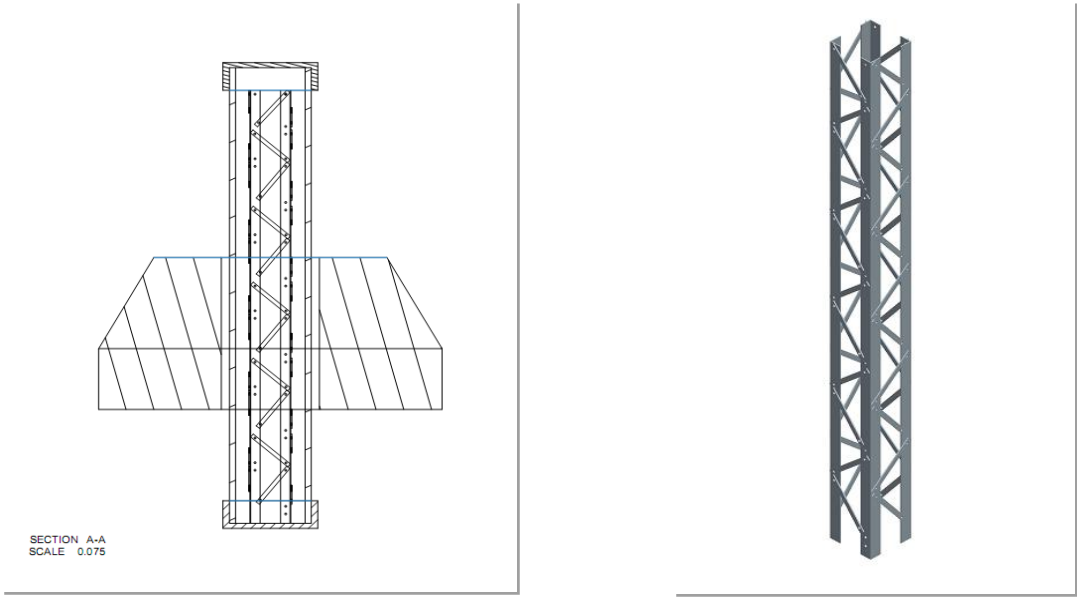

Figure 9: The photo on the left is a cross section of the spar buoy, exposing the interior cage. The picture on the right is a three-dimensional model of the interior cage. Both models were made in ProEngineer.

All components of the hydraulic power take-off system for the WEC are housed within the central spar buoy and mounted on the internal cage as seen in Figure 9. The inner cage supports the hydraulic system, and is made from high carbon steel angle irons and strips. Before this buoy can be deployed, the generator needs to be completely water tight, we considered the best way to do this was with spray foam. Although spray foam would be difficult to remove, it would be inexpensive and would be relatively water tight. Also gaskets between the piston shaft and the hole in the spar buoy plug would be added in order to prevent water leaking into the power take-off system.

4.0 Experimental Methods

4.1 Motor Calibration

The motor calibration allows us not only to validate our angular frequency outputs for other tests; it allows us to easily convert from voltage to frequency. The testing began by securing the motor. The motor was mounted to a 12x36x1.5 inch board, and then connected to a 50Amp power supply. A multimeter was used to determine exact voltages from the power supply and a tachometer was used to determine the angular velocity of the shaft on the motor. Data was collected for shaft speed by keeping the amperage constant and varying the input voltage from one to fifteen volts, then the data was plotted and an equation was determined for shaft velocity as a function of input voltage using a linear line of best fit.

4.2 Time Response of the Motor

From the time response of the motor the time constant of the system was also determined; this was important because it is used in the Matlab Simulink theoretical model, as a system parameter, and contributes to the system response. The DC motor and a brake were the bolted to the test mount to prevent movement. The brake and the motor were coupled, as seen in Figure 10, so that the brake would apply a resistance to the motor while it was rotating.

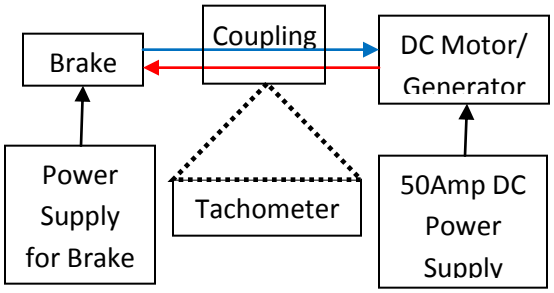

Figure 10: Experimental Set-up for motor time response. Photo on the left is a portion of the actual set-up for the system, and the diagram of the right shows a pictorial representation of the experimental set-up.

In the diagram on the right of Figure 10, there is a pictorial representation of the experimental set-up. The red arrow shows the torque being applied to the brake from the generator, the blue arrow shows resistive torque being applied to the motor, and the black arrows show the electrical power being applied to the brake and the DC motor, and the dotted lines show where the tachometer was reading shaft velocity. An Astron 50Amp variable DC regulated power supply was used to power the DC motor. A tachometer was then focused on

the shaft of the motor, and was used to determine the time at which the motor reached steady state.

Figure 11: Experimental set-up for motor time constant, showing where the tachometer sits to read the shaft speed.

Time was recorded using a stop watch, and using iteration more values that fit a first order time response curve were determined. A separate DC power supply was used to power the break, allowing the load on the break to be varied. Table 1 displays the settings used for this experiment.

	Amperage (Amps)	Voltage(V)
DC Power Supply for Motor	50	10
DC Power Supply for Break	10	0, 1.08, 3.02, 5.56

Table 1: The table above shows the power supply setting for both motor and break during the testing for the motor time constant.

Using the setting in Table 1, data for the damping of the motor was collected, and was used to find the damping coefficient. The damping coefficient was determined based on the collected data. The tachometer being used had no dynamic memory so it was impossible to generate a proper time response curve this is why a stop watch was used. The resistance on the shaft was varied by changing the voltage input into the brake, causing more or less resistance on the shaft of the motor. Plots of time vs. shaft speed can be plotted in order to determine the damping of the motor.

4.3 Time Response of Hydraulic System & Pipe Resistance

The hydraulic system was tested to find the resistance and capacitance values used in Equation 7 and modeled using Matlab Simulink, as well as to compare the output voltage of the system to those theoretical values calculated using the Simulink model. In order to test the hydraulic system it would be desirable to use the hydraulic piston and to input a displacement at a frequency resembling sea state. Problems arose with this concept though, it was difficult to

generate the force required to drive the piston at the low frequencies need with the equipment available. Due to these limiting factors the piston was replaced by an AC hydraulic pump. The pump had a throttle value on the outlet that was used to change the flow rate through the system. By using a motor instead of the piston the input to the system would be changed dramatically. When using the piston there would be a periodic input into the system while the motor would be a constant input after it reached steady state. These differences are another limiting factor in the modeling of the WEC system. Figure 12 shows a diagram of the benchmark test, where the arrows represent the hydraulic pipes between elements.

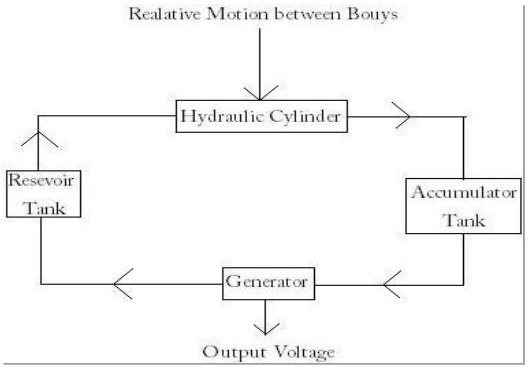

Figure 12: Diagram of experimental set-up.

Vegetable oil was used instead of hydraulic fluid, for the working fluid for the benchmark tests. There are some advantages for using hydraulic fluid as a working fluid as opposed to other fluids; for example hydraulic fluid has antiwar characteristics, corrosion control, minimizes internal leakage, and is fire resistance. Most of these characteristics are not necessary for this project, for example when deployed the buoy will be in the Atlantic Ocean surround by cold water, this will significantly reduce the chances of a fire in the hydraulic system. Deployment will also only be for a short amount of time, a few hours or days at most, so wearing and corrosion are not a large concern. Vegetable oil was chosen for two reasons; it is low in cost, and is environmentally friendly.

Data for flow rate and pressure drops were required to complete the theoretical model of the system. Flow rates were taken by connecting a GE Transport PT878 Ultrasonic Flow Meter; the flow meter measures the flow rate of acoustically conductive single-phase fluids. The PT878 is a transit-time ultrasonic flow meter. When ultrasonic pulses are transmitted through a moving fluid, the pulses that travel in the same direction as the fluid flow travel slightly faster than the pulses that travel against the flow. The PT878 determines the transit times and then uses the transit time to calculate the fluid flow velocity. The flow meter provides an analog output of flow velocities or volumetric flow rates. The measured volumetric flow rate, Reynolds number and fluid velocity are available from the PT878 Ultrasonic flow meter. The flow meter needs a solid pipe to connect to the system in order to have accurate

readings (per PT878 flow specification flow Accuracy typical +/-2% or +/-0.03ft/s), since the hydraulic line consists of braided steel wire coated with nylon a galvanized steel nipple was installed between the inlet and exit of each element of the system to permit the installation of the PT878 Ultrasonic flow meter. Two transducers were installed on the nipple at a calculated distance based on nipple material, diameter and the working fluid properties. The calculated transducer separation of 1.079 inches apart was determined by the PT878 flow meter; this number was calculated by the flow meter according to the pipe characteristics stated above. A hydro coupling gel is used between the transducer and the piping to insure that there is good contact with the surface of the pipe to permit the travel of sound waves.

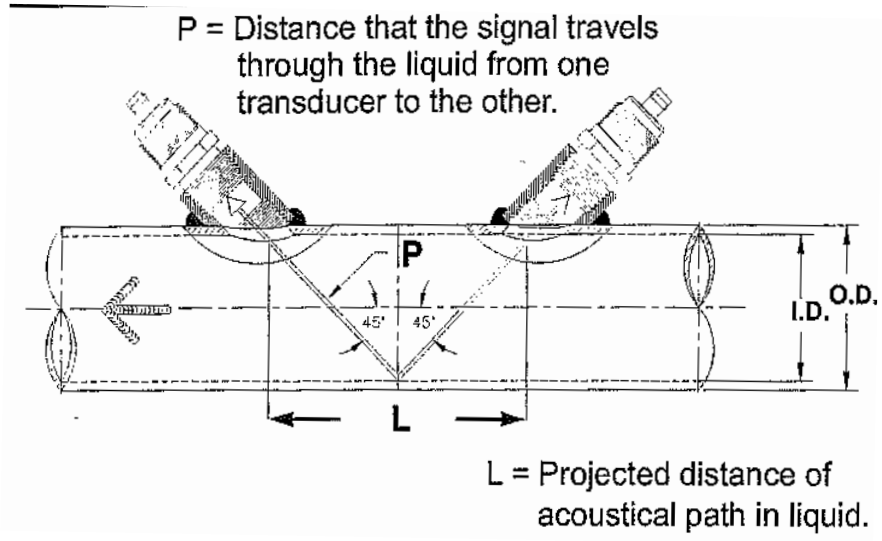

Figure 13: Shows a diagram of how the flow meter transducers work on a pipe.

A t-fitting was attached to each of the nipples, so that a pressure transducer could be attached, allowing pressure measurements to be taken at the inlet and exit of each element. The data was collected using a Sensym ST2300G1 pressure transducer and a voltmeter. The pressure transducer could read pressure between 0 and 300psi. Using the calibration for the transducer, output voltages were converted to pressure (psi) allowing the pressure drop across each of the system components and hydraulic lines to be found. The added fittings and nipples did cause some additional pressure drop throughout the system, due to minor losses between transitional zones. These pressure drops, although small, may cause error when comparing the results from the actual WEC, when deployed, to the theoretical and benchmark tests.

Figure 14: Hydraulic system, benchmark testing area. The photo on the left shows the entire hydraulic system with the pressure transducer attached in front of the generator. The photo on the right shows the flow meter used to take the volumetric flow rate during the testing.

Figure 14 is a photograph of the hydraulic benchmark test set-up. The reservoir tank can be seen inverted in the left photo. This photo was taken before the system was running, but the basic placement of the elements is the same.

The resistance in the piping can be found similarly to the way that you find the resistance in an electrical circuit. In a fluid system the current would be analogous to the flow rate of the fluid and the voltage drop would be represented by the pressure drop. Now using the following equation, the resistance can be calculated;

$$r = \frac{\Delta P}{Q} \ , \tag{12}$$

Where Q is the mass flow rate, and ΔP is the pressure drop though the pipe, P_{in}-P_{out}.

To determine the power output from the generator the electrical output of the system was connected to a load bank. The load bank consisted of twelve three ohm resistors in parallel that could be activated individually. The flow rate of the system was held constant while the resistance was altered. After recording measurements for all resistance values the flow rate was modified and the process was repeated. Readings were taken for a total of five different flow rates and twelve different resistance values.

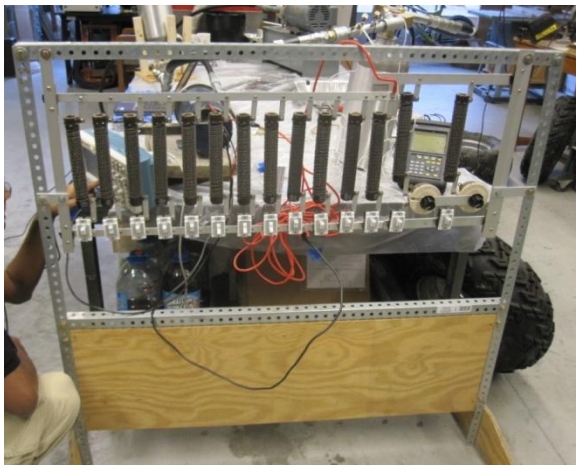

Figure 15: Shows the load bank used during testing to find the power output of the system.

Using Ohm's Law in conjunction with the equation for power of an electrical system it is possible to take the recorded values of voltage and resistance and determine the power,

$$v = I * R, \text{ or } I = \frac{v}{R} \tag{13}$$

Equation 13 states that the voltage, v, is equal to the current, I, multiplied by the resistance, R. Then the using the relation that power equals current times voltage and substituting Equation 13 into the power equation it is possible to determine the power output with measured data,

$$P = V * I = \frac{v^2}{R} \tag{14}$$

This data was then plotted and a power versus resistance plot was generated, this plot is shown in Figure 22 of the report.

5.0 Experimental Testing

The goal of this project was to model the hydraulic system and the generator, to determine the dynamic response of the Wave Energy Converter, or the WEC, system. To model these components testing was conducted to determine the necessary constants of the system. This involved multiple sets of testing on the total system, the hydraulic system and the generator individually.

5.1 Hydraulic System Test:

The first system considered was the hydraulic system. The objective was to characterize the flow within the hydraulic lines based on the volumetric flow rate within the system. The main concern was the resistance within the hydraulic lines. Based on the design of the system, it was determined that the resistance within the lines would be non-linear. In order to compensate for this fact, a model for the resistance was created based on volumetric flow rate.

To determine the characteristics of the flow of the system, the piston was replaced by an electric pump so there would be a constant flow rate moving through the system. The pump was a 120V AC pump with a reservoir and a throttle valve on the outlet. The throttle valve was used to vary the flow rate by either restricting or opening the outlet of the pump. The flow rate was measured using an ultrasonic flow meter, which inputs an acoustic signal through the flow of the system and then measures the shift and amplitude of the return signal to determine the flow rate of the system and other flow characteristics. The flow rate was varied from one to two gallons per minute (gpm), at different intervals. Pressure readings were then taken using a Sensym pressure transducer. Readings were taken at the inlet and outlet of every component in the system. This allowed pressure drops to be determined across all components for all flow rates. Knowing the pressure drops within the system it was possible to generate plots in determine resistance in the lines as a function of the flow rate using a modified version of Equation 12,

$$R = \frac{\Delta P}{\dot{Q}} = \frac{\Delta P}{\rho \dot{V}}, \tag{15}$$

Using Equation 15 it was possible to determine a resistance value for each of the flow rates. Then by plotting these resistances against the flow rate of the system and applying a line of best fit it was possible to determine an equation for the resistance values based on the volumetric flow rate of the system.

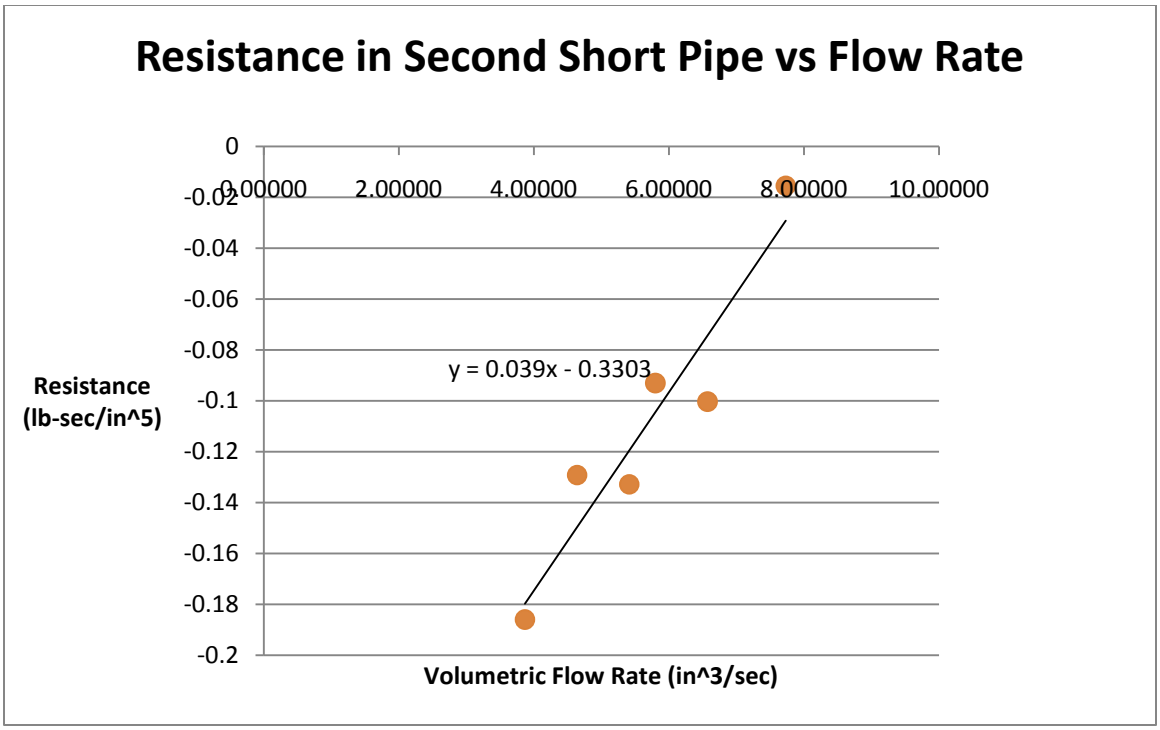

Figure 16: Shows a plot of the resistance values calculated for the short section of hydraulic line between the generator and the reservoir tank. The black line shows a linear fit for the resistance in the pipe. Resistance plots for all other pipes can be found in the appendix.

This process was then continued for each section of hydraulic lines and the components within the system. By using the equations generated by the line of best fit, the non-linearities of the system are compensated for, which allowed the hydraulic system to be modeled using Matlab Simulink.

5.2 Total System Response:

To determine the dynamic output of the total system an oscilloscope was used to measure the voltage output of the motor as it reached steady state. This allowed a time response to be obtained to determine the characteristics of the total system.

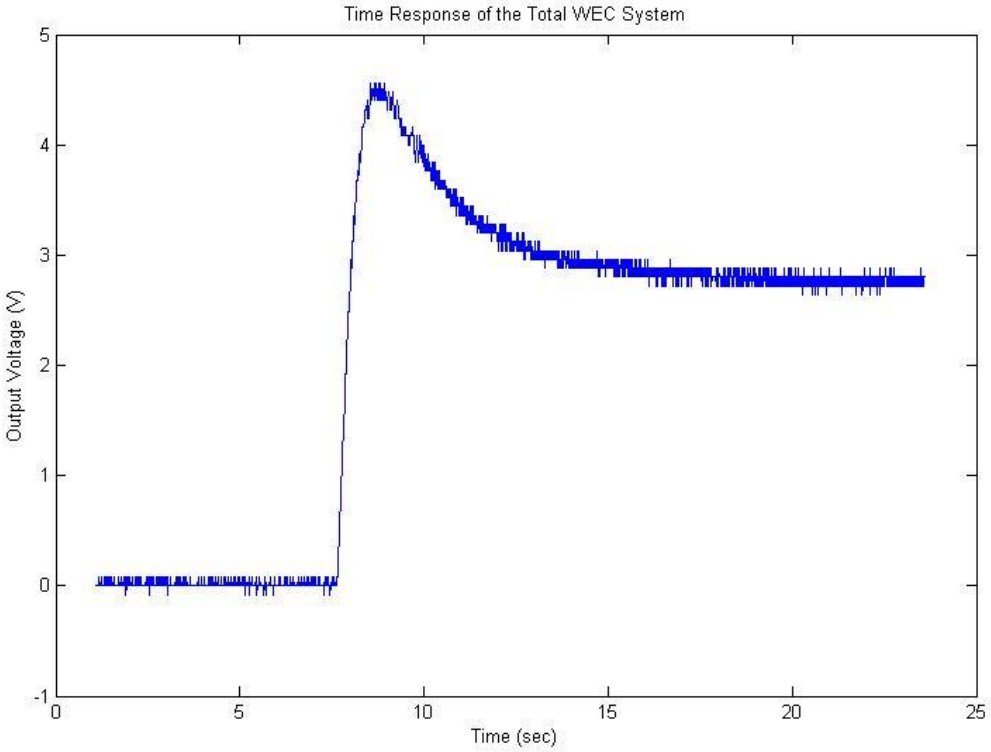

Figure 17: The plot above is the time response of the total system.

Figure 17 shows the response of the total system. The system behaved as a first order system decaying to a steady state value. The system started at zero voltage and remained there for approximately seven seconds while the system built pressure. After accumulating enough pressure to rotate the shaft of the motor the output voltage spiked, almost instantaneously, and then settled to a steady state of approximately three volts at approximately twenty seconds. Simplifying the input from the pump as a step input it was possible to analyze the response as a first order system. By analyzing this system as a first order it was possible to determine the time constant for the system and how it functions under ideal conditions with a pump applying a constant flow rate.

5.3 Ideal Motor Data:

With the total system considered the next step was to determine the response and the operating characteristics of the generator. Generator data was provided by the manufacturer which allowed some conclusions to be drawn, including the motor efficiency as a function of rotational shaft speed, seen in Figure 18.

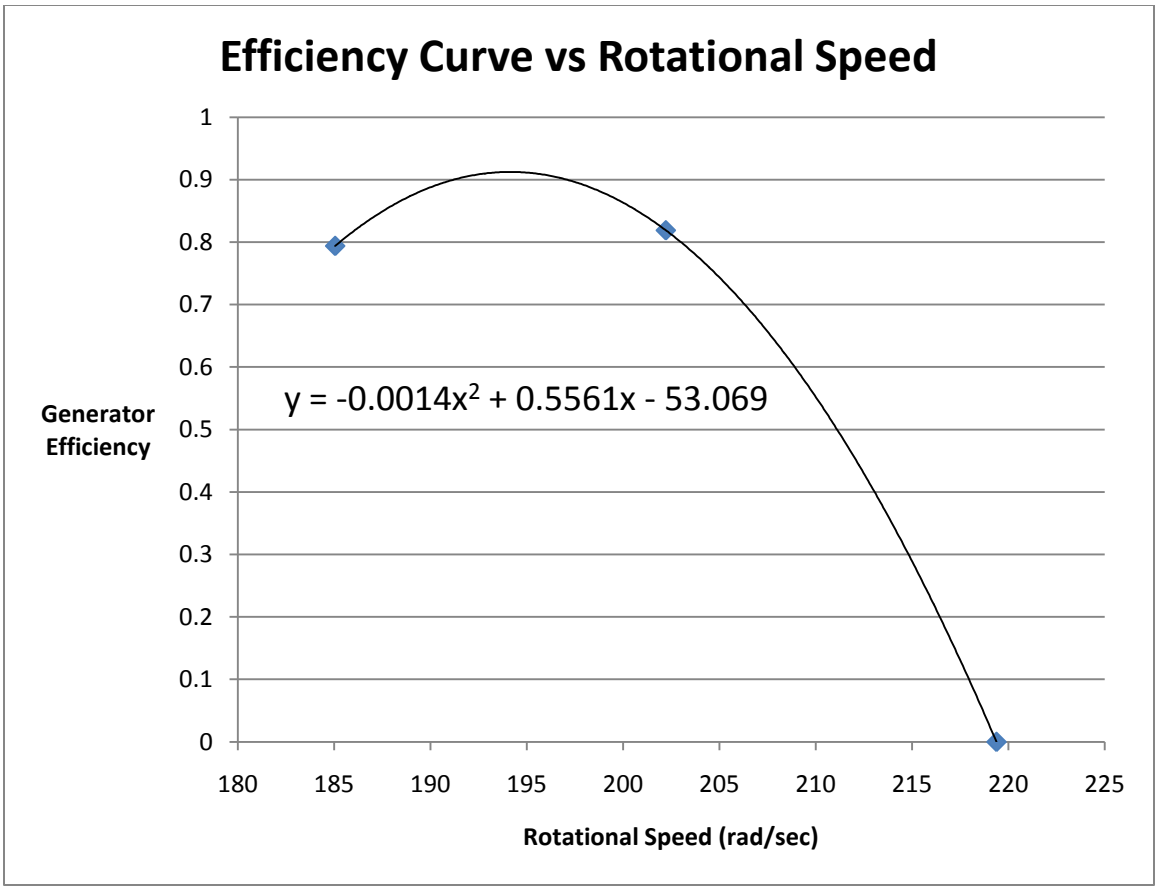

Figure 18: The plot above is the efficiency versus the rotational speed; this data was supplied with the motor.

Using Figure 17 it was possible to determine the efficiency based on the shaft speed. A maximum efficiency of approximately 0.91 is achieved at a rotational speed of 195 rad/sec, or approximately 1800 RPM. The plot showed that for a high or reasonable efficiency the rotational speed of the motor has to be relatively high. This was because the power for a rotational system was defined as,

$$P = T * \omega, \tag{16}$$

Equation 16 states that the power of the system is equal to the torque of the system multiplied by the angular velocity. To fully understand this relation a plot of output torque versus rotational speed was generated using the motor data provided by the manufacturer.

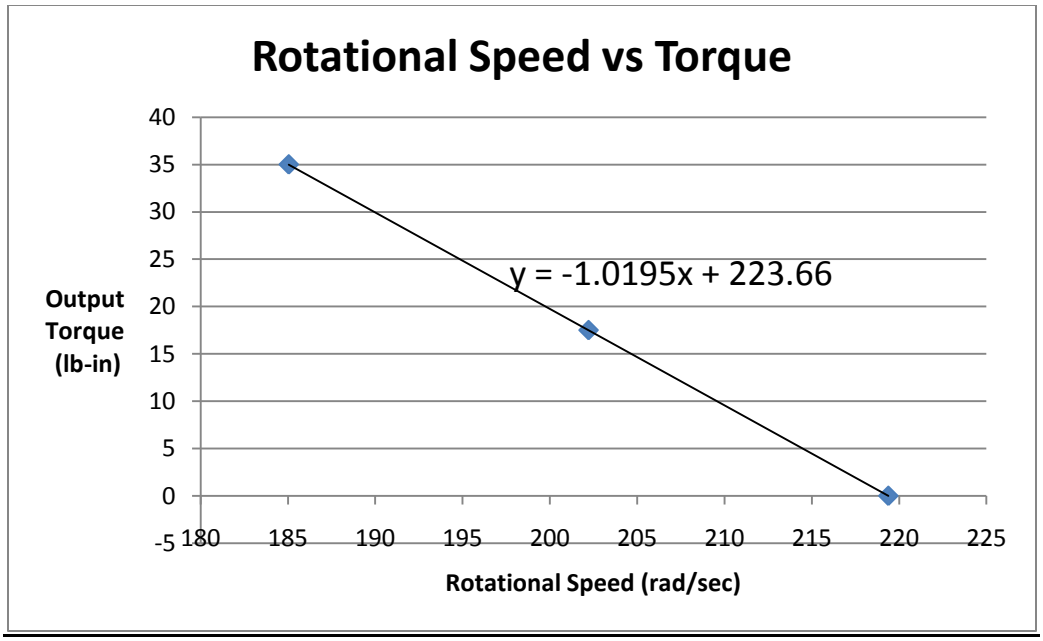

Figure 19: The plot above is the rotational speed versus torque; this data was supplied with the motor.

Figure 19 was used to determining the characteristics of the generator being used and to how it functions within the total system. It also helped to judge whether this generator was a feasible design choice based on the system.

5.4 Generator Testing:

To properly model the system using Matlab Simulink generator constants needed to be derived through testing. To derive the constants multiple tests were conducted, the first was a zero load test. The motor was attached to a 50A power supply and the voltage was varied between two and fifteen volts, while the shaft speed was measured using a tachometer. A plot was generated using this data, and can be seen in Figure 20.

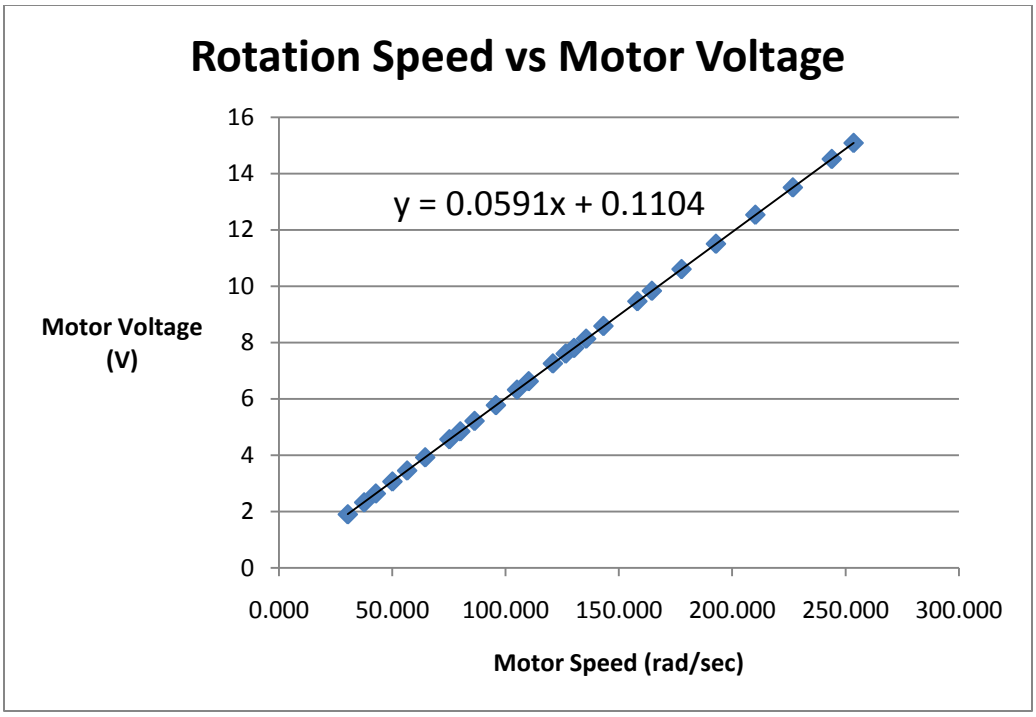

Figure 20: The plot above is the rotational speed versus motor voltage; this data was supplied with the motor.

Figure 20 shows the motor voltage as a function of the shaft speed. A line was then fit to this data where the slope of the line, 0.0591 V-s, is the motor constant, K, for the generator. Next a similar process was used to obtain a time response for the generator. Since there was no way for the shaft speed to be measured dynamically a tachometer and a stop watch were used to determine the time response. The generator started at zero shaft velocity and then a voltage was applied; the shaft speed was then recorded until it reached steady state when the time was recorded from the stop watch. This allowed a time response to be generated assuming that the generator behaved as a first order system.

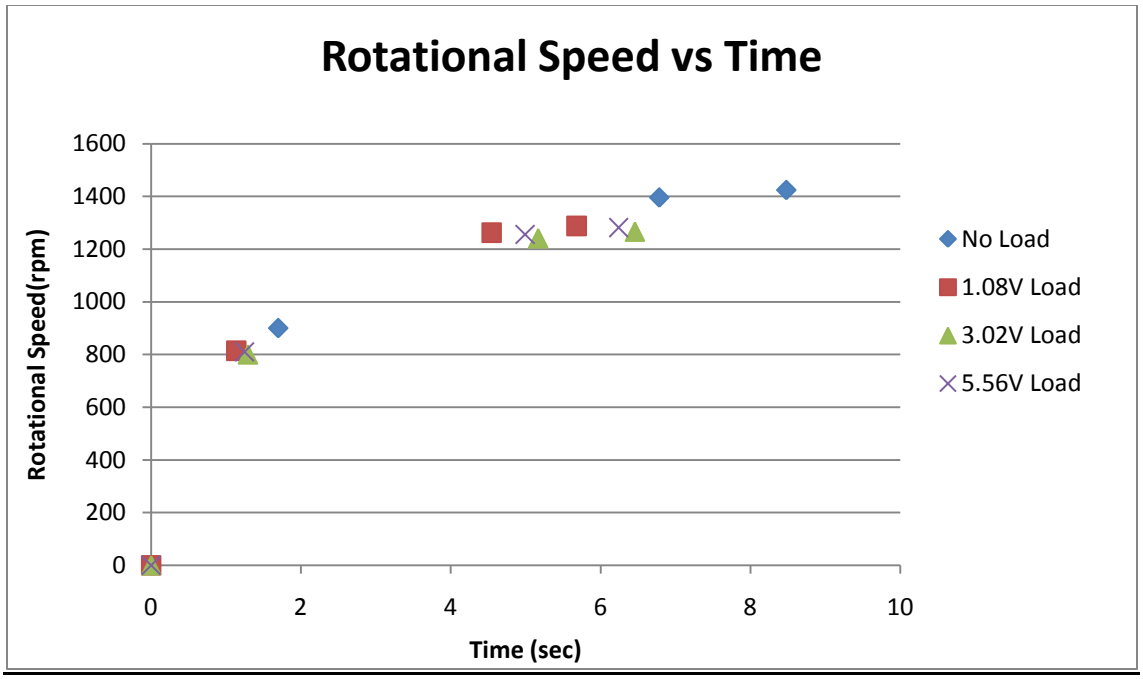

Figure 21: The recorded rotational speed versus time for four different loads applied to the break from 0 to 5.56V.

Figure 21 allows the time response of the generator to be calculated. The time constant was determined to be approximately 1.5 seconds. Next, load data was taken for the system. The total system was reconstructed with a constant input source coming from the pump. The output of the generator was then attached to a load bank. The resistances were then varied to determine the power being generated over different resistance values. The voltage was measured using a voltmeter and then the power was calculated using Equation 14. Using Equation 14 it was possible to generate a plot of output power as a function of the resistance across the output device.

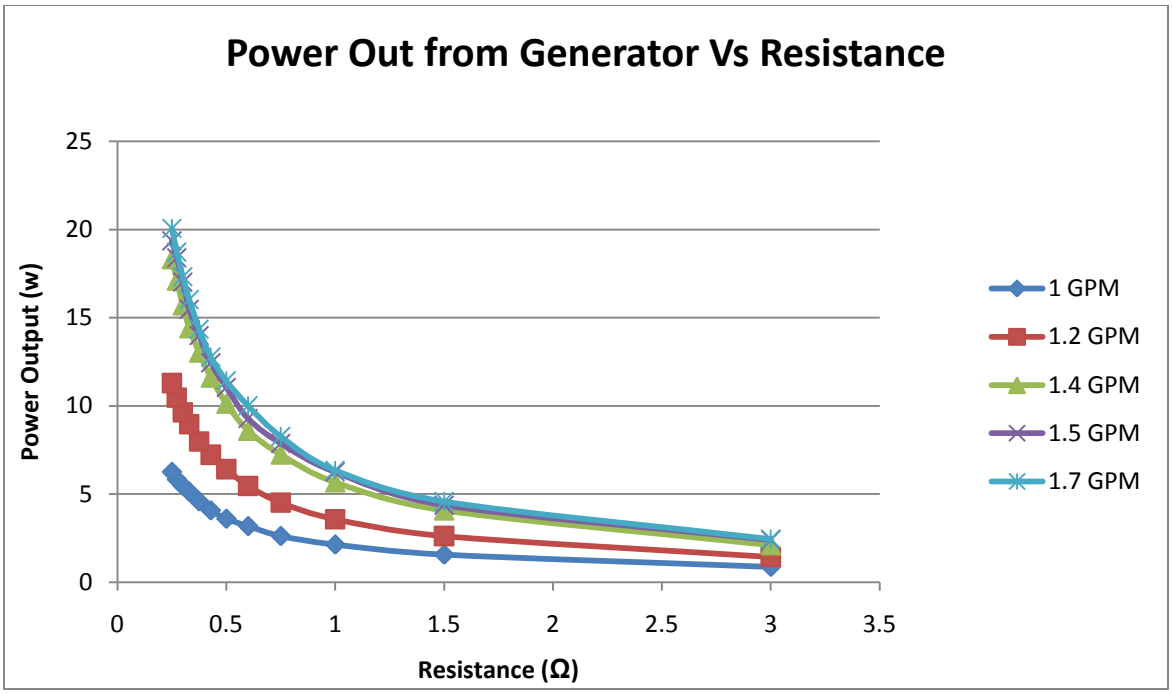

Figure 22: Plot of the output power from the generator versus the resistance across the load bank for five different flow rates between 1 to 1.7GPM.

Figure 22 shows that when the resistance of the output device increases the power output of the system decreases.

5.5 Simulink Results

After gathering the results from previous testing it was possible to apply the constants to generate a Matlab Simulink model for the hydraulic system. A model previously generated by James Wright was used. The input functions and the motion equations for the Simulink model were still applicable. Only the constants of the equations needed to be modified in order to scale the waves from a lower scale model into a more lifelike model with reasonable wave amplitudes and periods. Two different wave types were generated using this data an idealized sinusoidal wave and a representative sea-state wave using the Bretschneider spectrum.

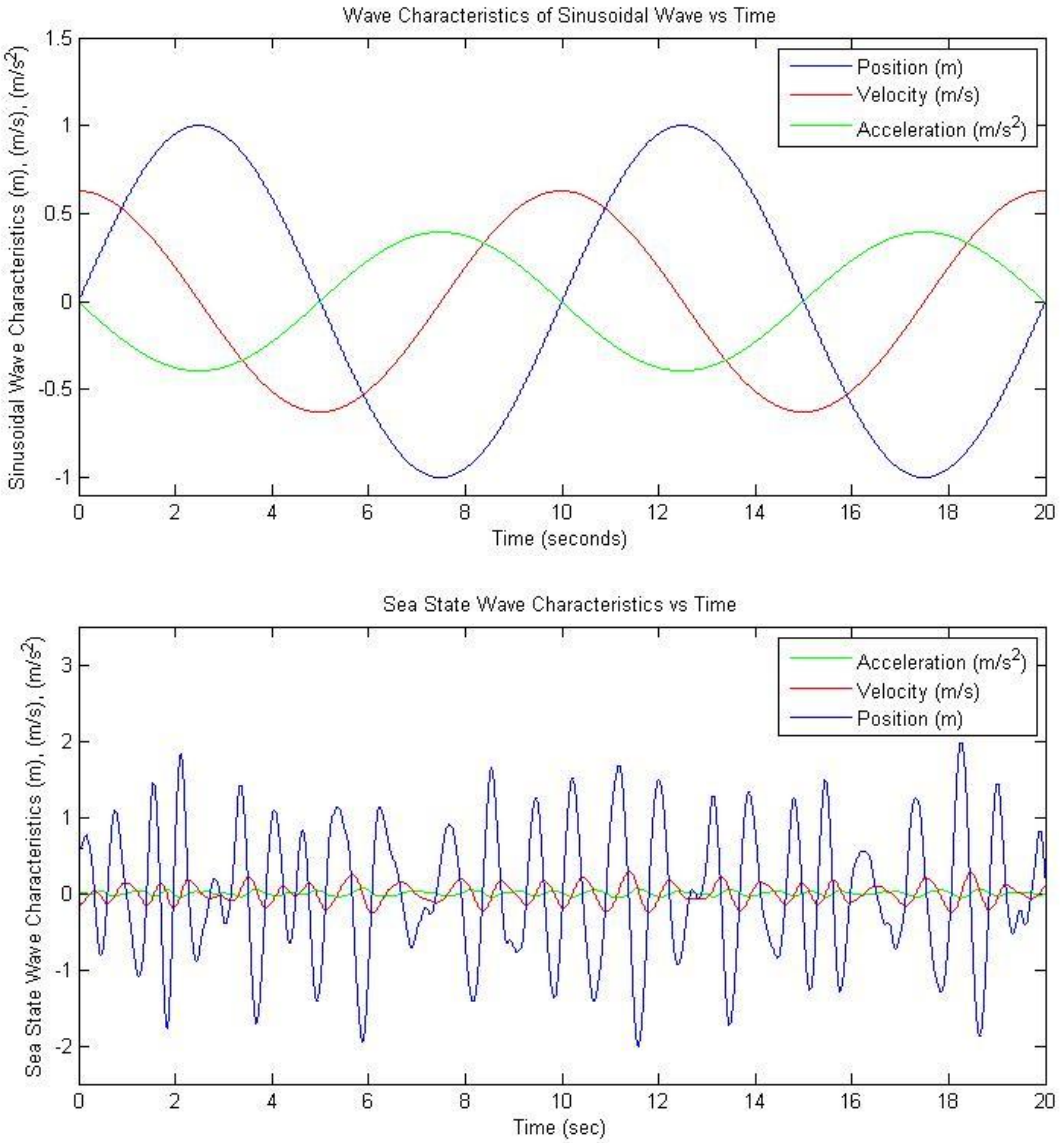

Figure 23: The wave position (m), wave velocity (m/s), and wave acceleration (m/s2). The top graph is for a sinusoidal wave input, and the bottom plot is for a random sea state wave input.

Figure 23 shows wave position in meters, wave velocity in meters per second as well as the wave acceleration in meters per second squared. As can be seen there are some significant differences in the wave characteristics. From these inputs the Simulink model then determines the displacement of the spar buoy and the follower buoy and then combines them to determine the relative displacement of the buoys.

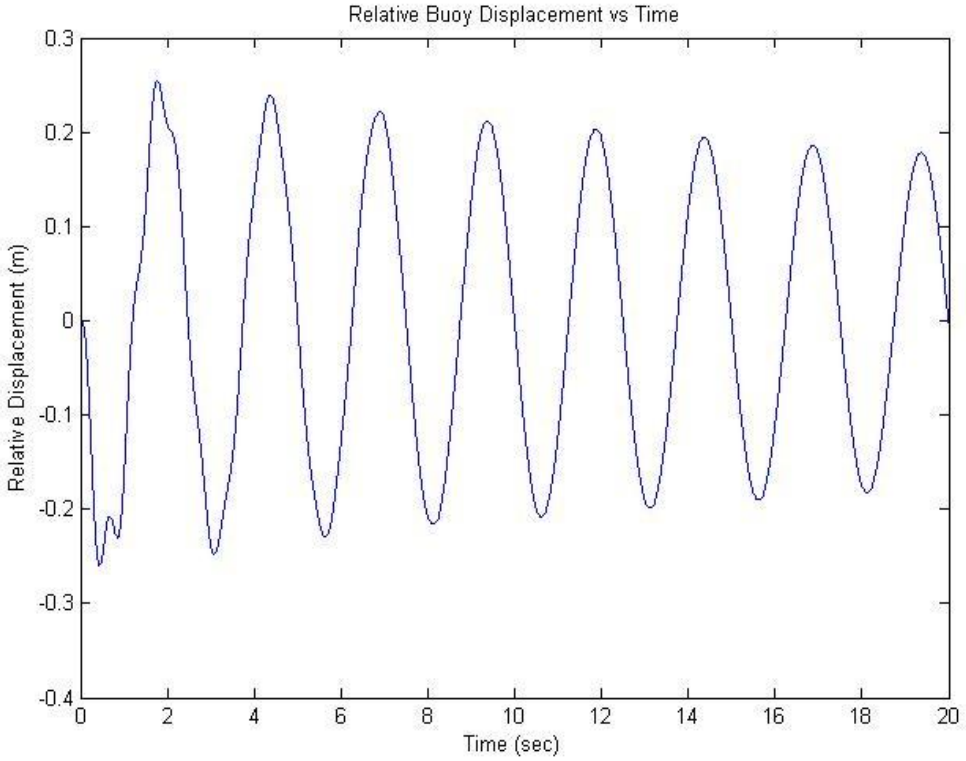

Figure 24: The relative displacement (m) of the spar and follower buoy for the Sinusoidal wave spectrum. Relative displacement for the sea state waves is included in the appendix

Figure 24 shows the relative displacement for a sinusoidal wave input into the Simulink system. The plat started off slightly irregular then reached a sinusoidal state that was gradually decaying.

Next the hydraulic take off system was considered. The differential equations for the hydraulic system were written with respect to volumetric flow rate. To determine the flow rate the first derivative of the relative displacement was considered. By multiplying the relative velocity of the system by the cross-sectional area of the piston the volumetric flow rate was determined. This flow rate was then used as an input into the resistance equations derived experimentally to solve for the angular velocity being output by the hydraulic system. This angular velocity was input into the differential equation for the generator which was then solved to determine the power output of the system.

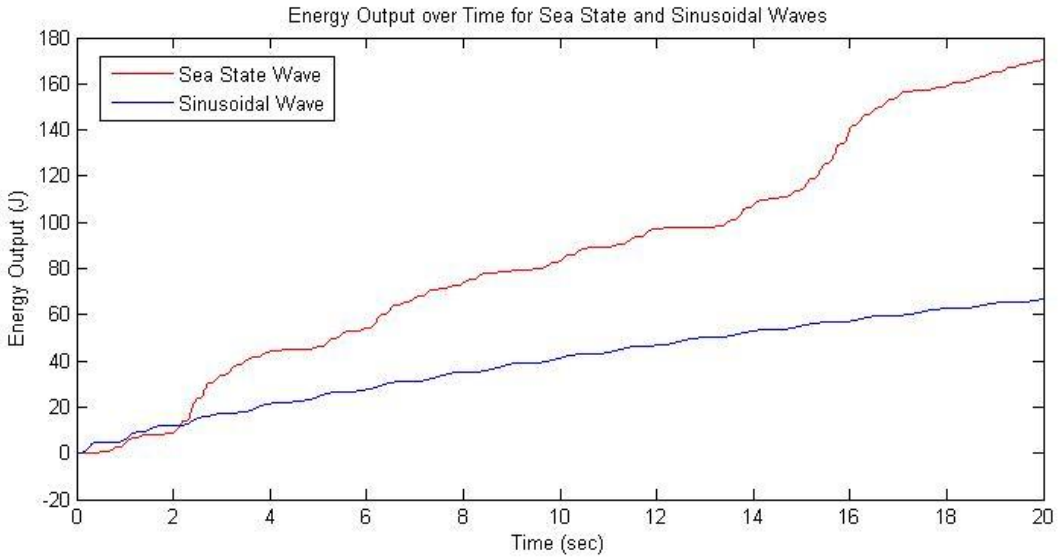

Figure 25: The plot shows the energy output over time for the sea state wave input (red) and a sinusoidal wave input (blue).

Figure 25, shows the energy output for both the sinusoidal wave and the sea state wave. The sea-state wave has a higher output energy compared to the sinusoidal wave, while the sinusoidal wave has a much steadier slope.

6.0 Conclusions and Future Work

Based on the testing performed and the results analyzed the hydraulic take off system is a feasible choice when designing a point-absorber buoy. Based on the total energy in a standard sea wave per area and the cross-sectional area of the follower buoy it was possible to determine the efficiency of the entire system. By taking a ratio of the power generated by the system, the energy output divided by the time, and the energy in a standard wave it was possible to plot the efficiency as a function of time.

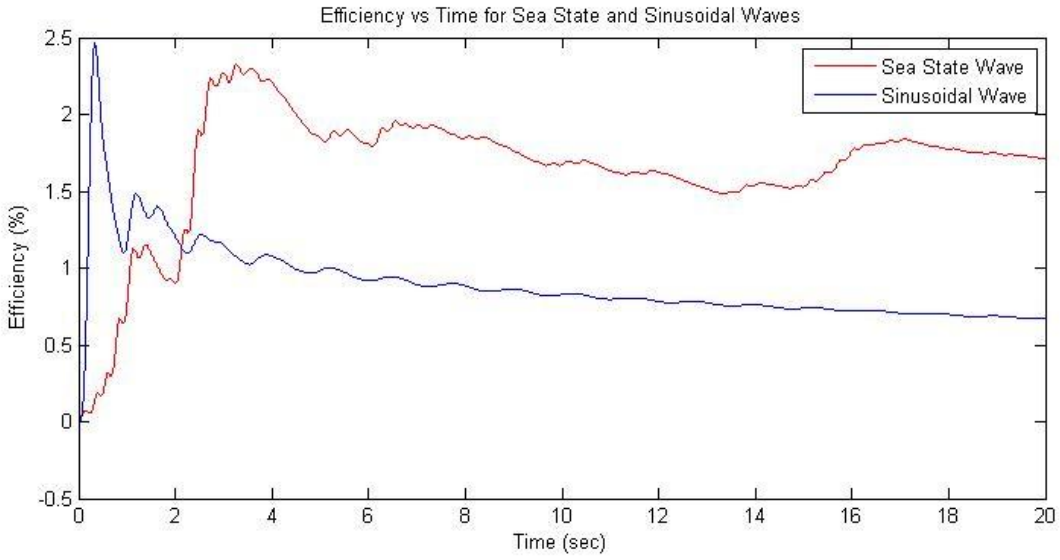

Figure 26: The plot above shows the efficiency of the hydraulic system over time for both the sea state input (red) and the sinusoidal input (blue).

In Figure 26 the sinusoidal wave approached a steady state efficiency of approximately 0.75% while the sea-state wave efficiency oscillated around 2%. The maximum efficiency for a wave capture device is 50%, and since this is a passive system the maximum expected efficiency dropped even lower to approximately 5%. So based on the analysis of the system an efficiency of 2% is reasonable given the operating conditions.

Seeing the testing results obtained and the functionality of each sub system showed the inferences that are limiting the output efficiency. Based on the testing and calculations performed in the project the most limiting component appeared to be the generator. Based on data obtained, plot of efficiency as a function of shaft speed, the size, rated power output of 1/2 horse power was limiting the tested system performance. In the system the generator reached angular speeds much below its desired functioning range, seen in the following Figure 27.

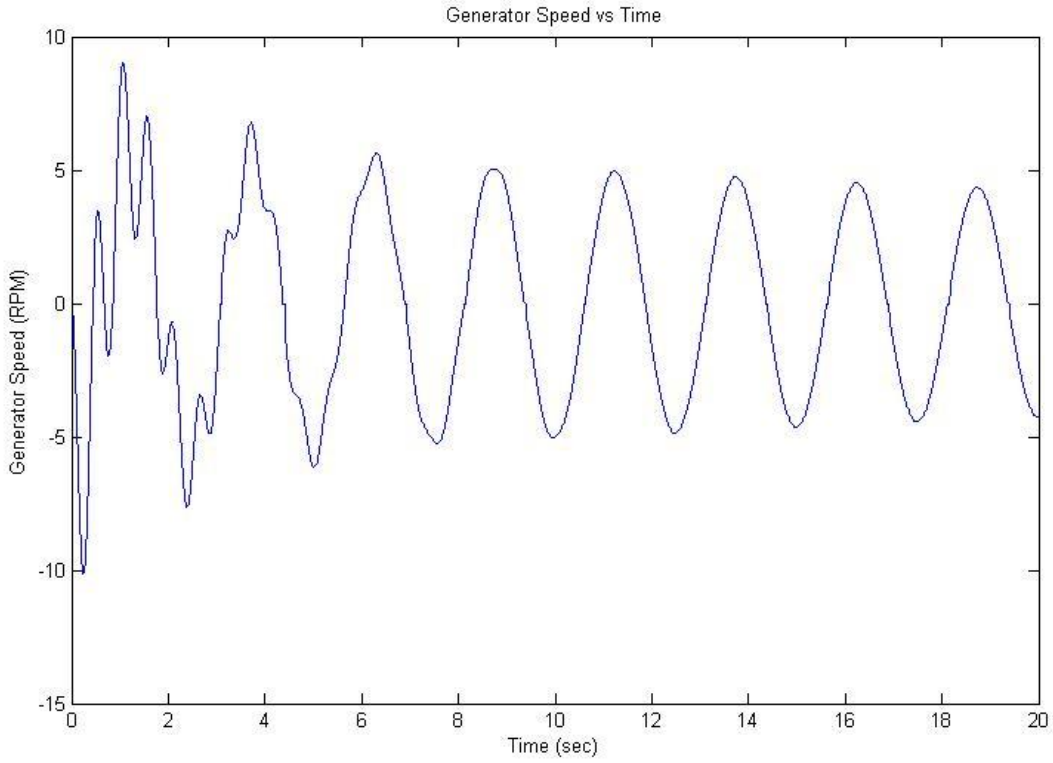

Figure 27: The plot above shows the speed of the generator over time for a sinusoidal wave case.

Figure 27 shows the shaft speed for the sinusoidal wave case, the RPM for sea state wave was attached in the appendices. In Figure 26, the plot the shaft speed at maximum reaches 10RPM and when the system reached steady state the angular speed approached 5RPM. This was far below the speeds needed for the generator to run with peak efficiency. Based on these results the generator being used currently has too large of a frictional torque value which in turn is causing the slow angular speed. If a motor with a lower frictional torque was used in the system that the output and the efficiency would increase.

References

Acheson, D. J. *Elementary Fluid Dynamics*. Oxford: Clarendon, 1990. Print.

Berteaux, Henri O. Buoy engineering. New York: Wiley, 1976. Print.

Dean, Robert G. Water wave mechanics for engineers and scientists. Englewood Cliffs, N.J: Prentice-Hall, 1984. Print.

Kenjo, Takashi. Permanent-magnet and brushless DC motors. Oxford: Clarendon, Oxford UP, 1985. Print.

Ogata, Katsuhiko. System dynamics. Upper Saddle River, NJ: Pearson/Prentice Hall, 2004. Print.

Appendix:

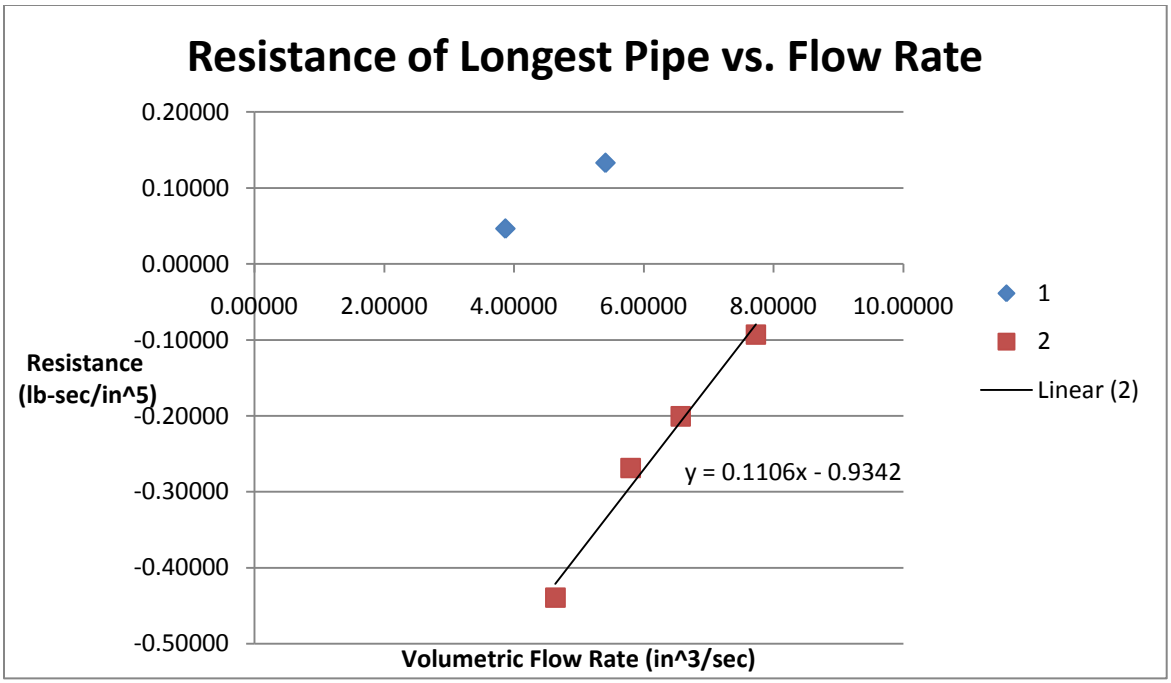

Figure A1: Resistance values in the hydraulic line between the piston and accumulator tank

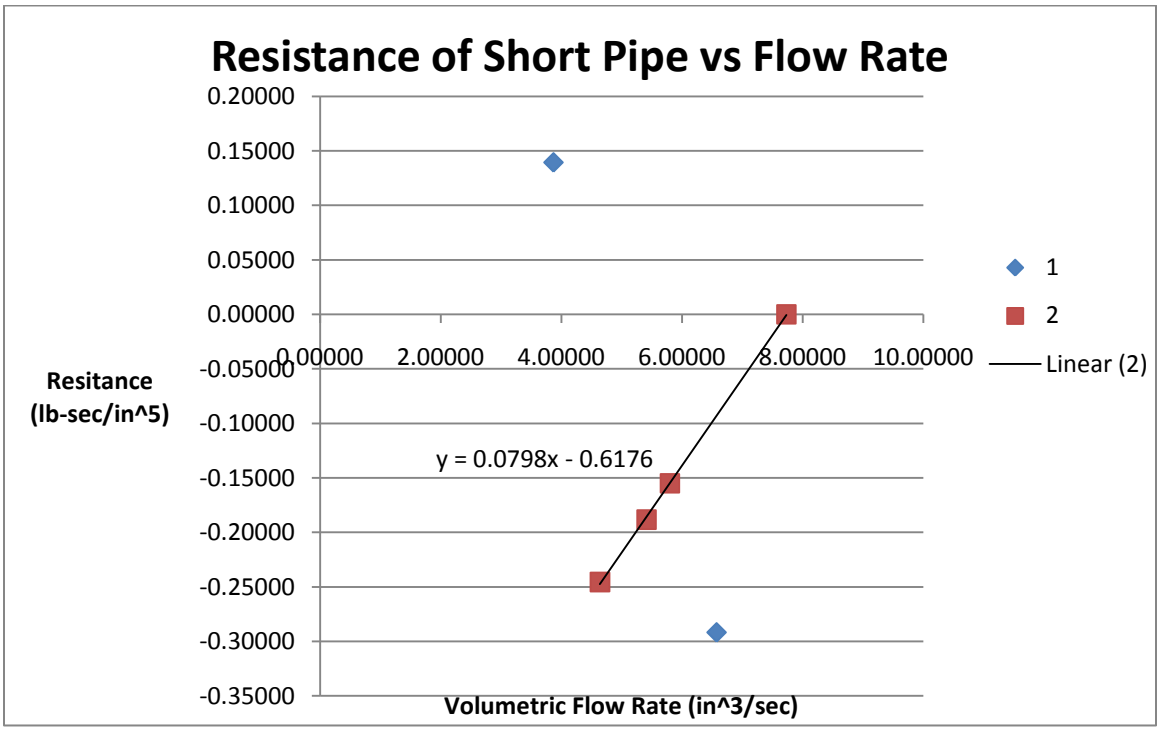

Figure A2: Resistance values in the hydraulic line between the accumulator tank and generator

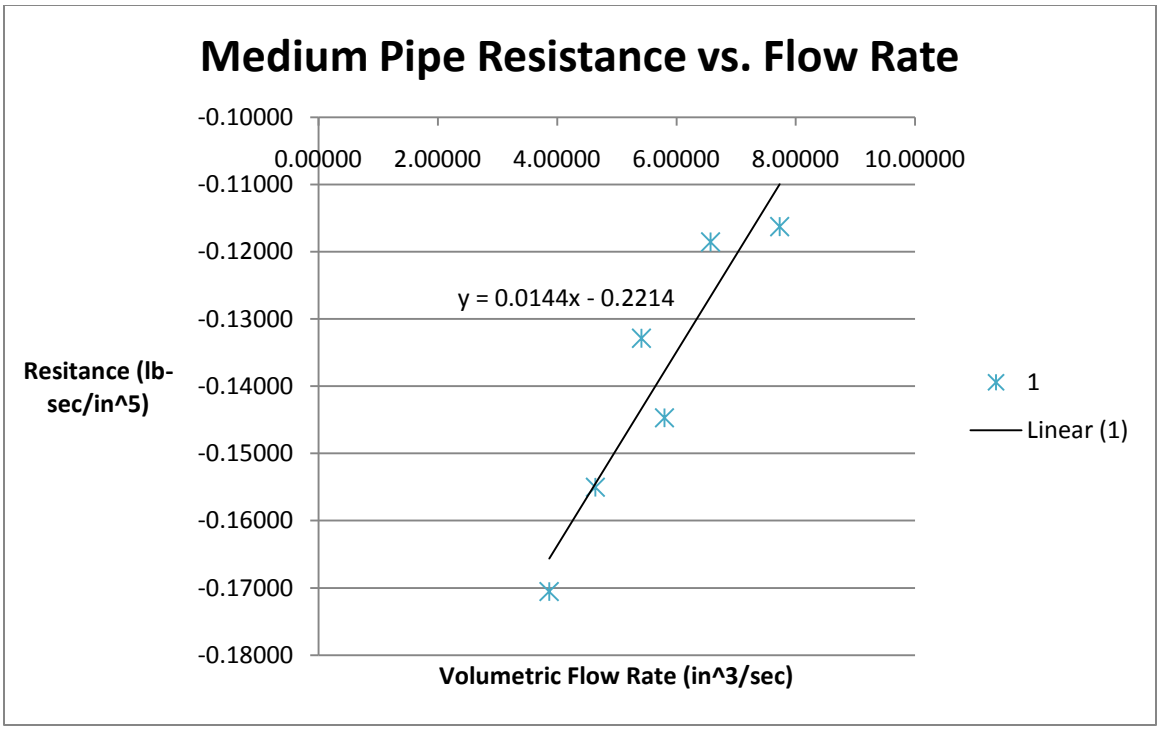

Figure A3: Resistance values on the hydraulic return line between the reservoir tank and piston

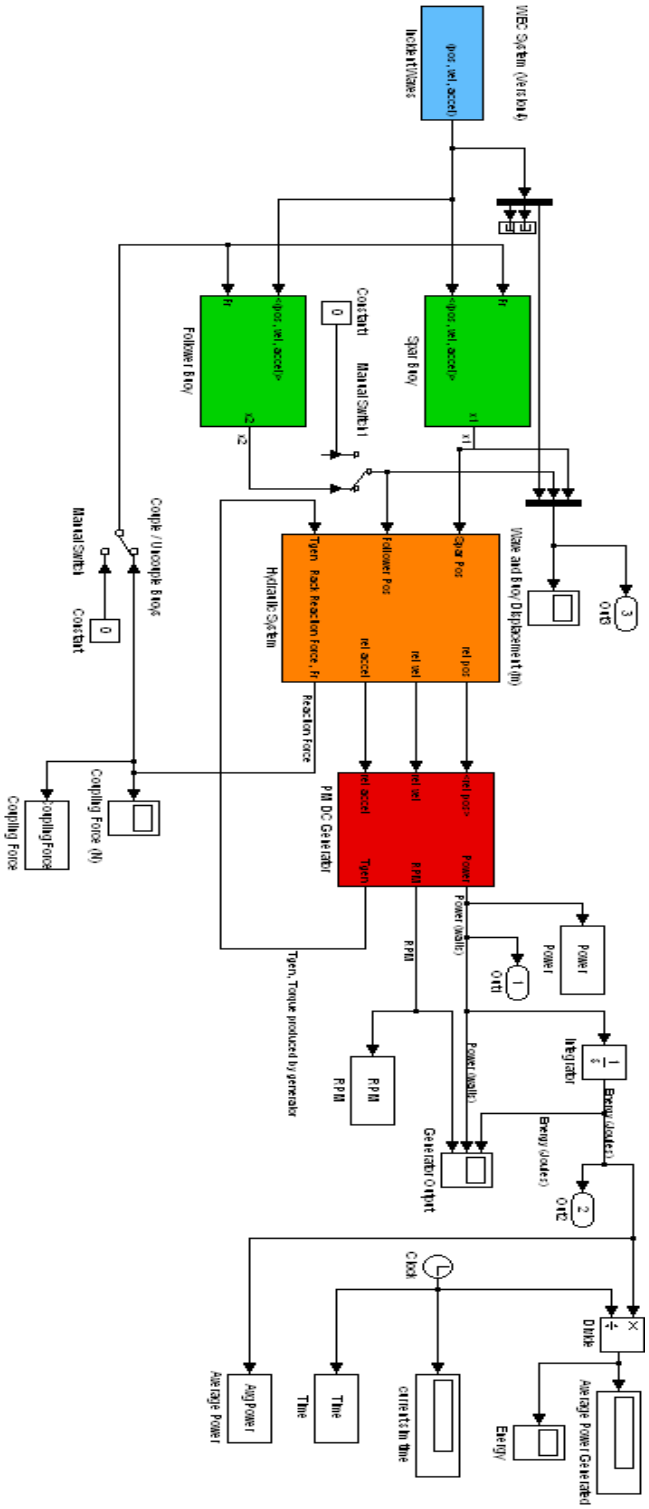

Figure A4: Model of Simulink program used to represent the WEC system

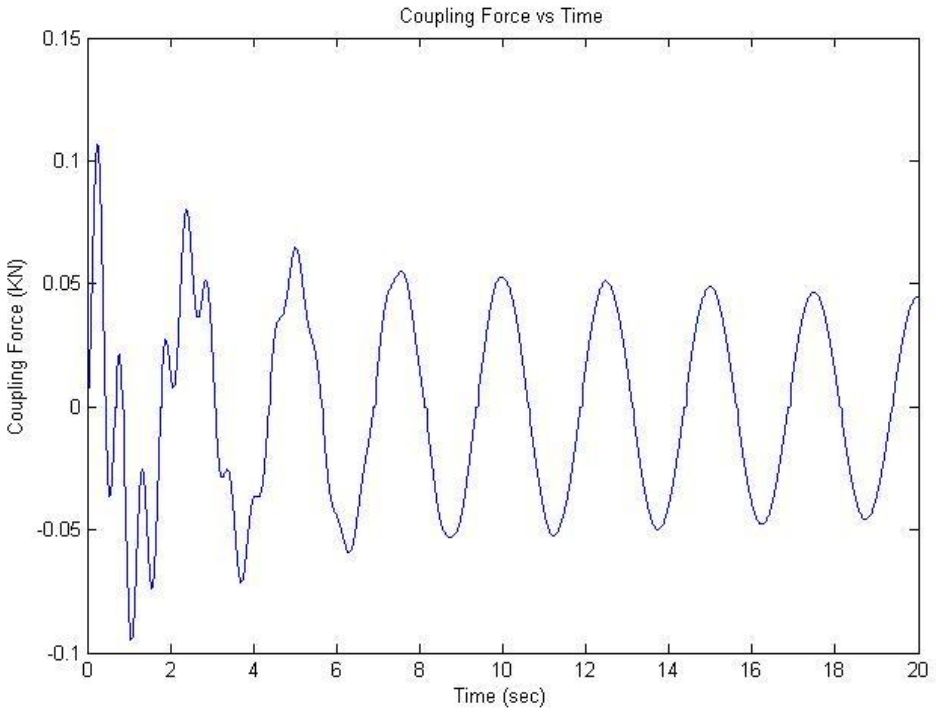

Figure A5: Coupling force between spar and follower buoy for a sinusoidal wave input

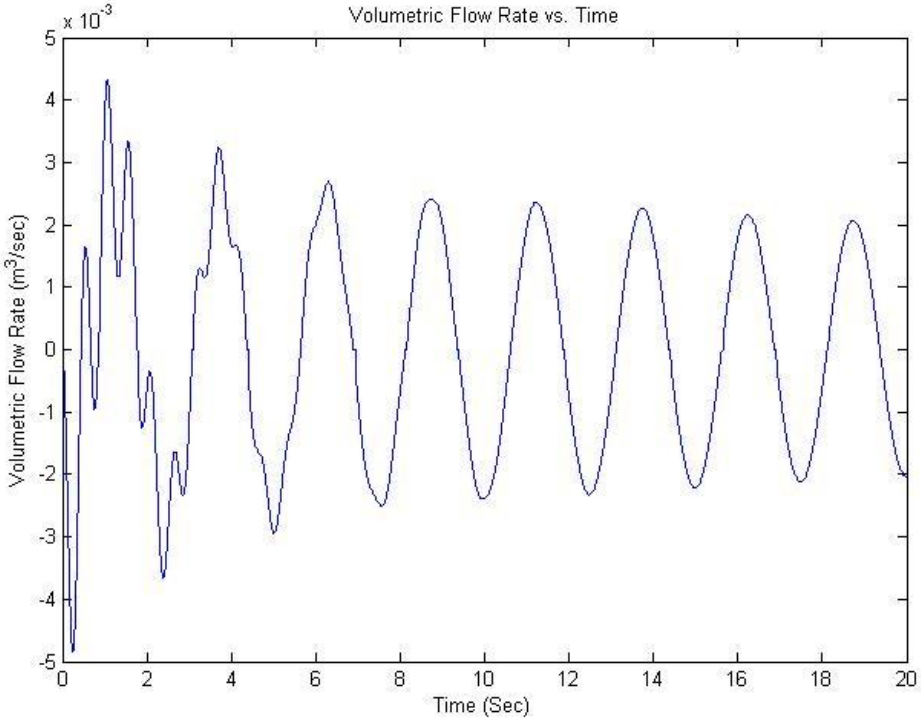

Figure A6: Volumetric flow rate of WEC system for a sinusoidal wave input

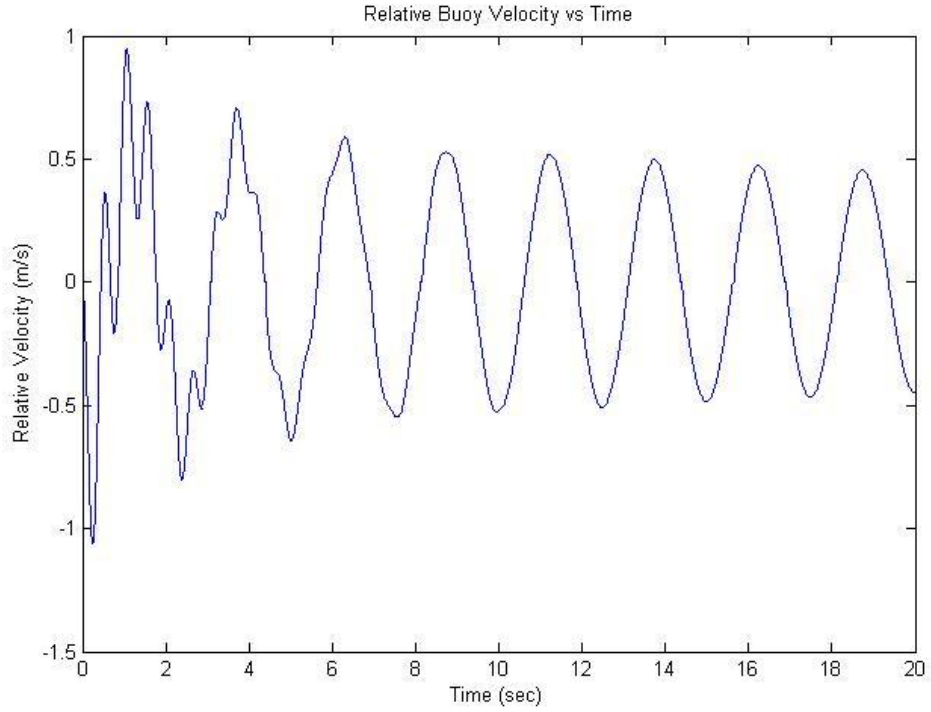

Figure A7: Relative velocity of WEC system for a sinusoidal wave input

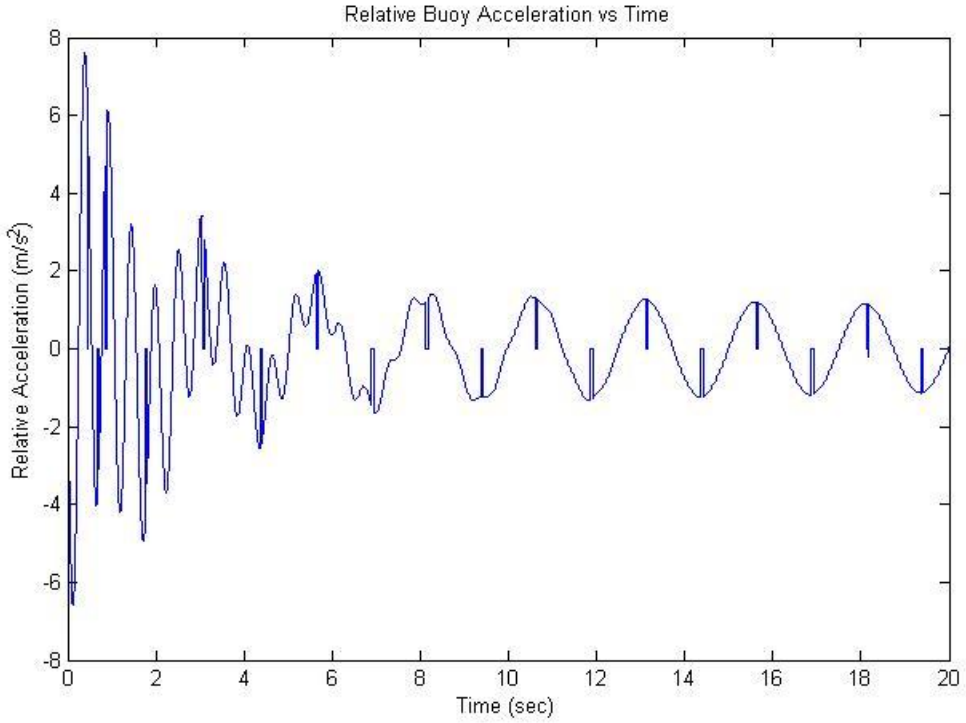

Figure A8: Relative acceleration of WEC system for a sinusoidal wave input

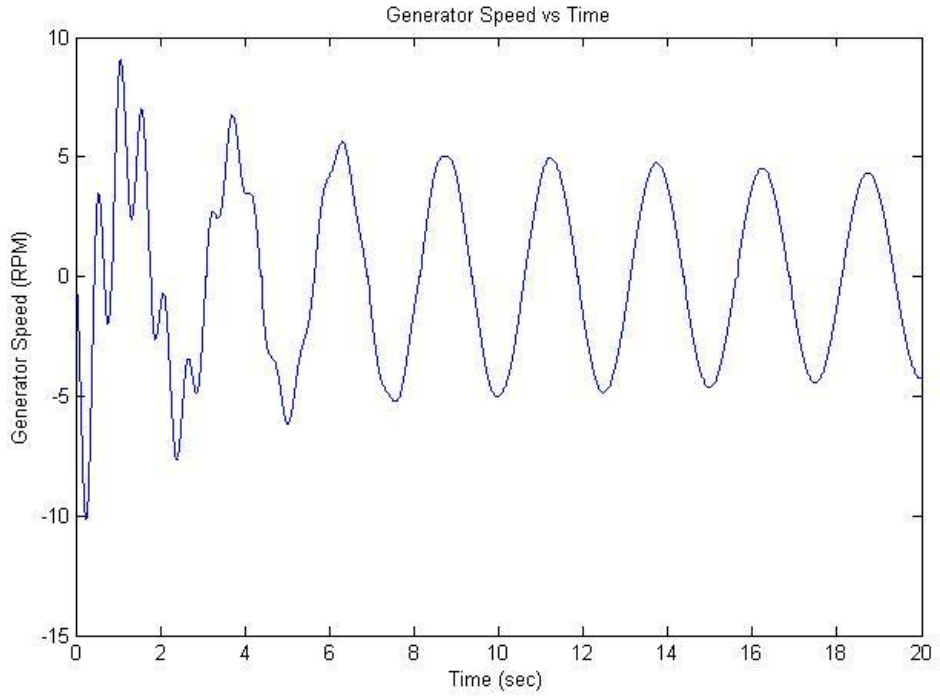

Figure A9: Generator shaft speed of WEC system for a sinusoidal wave input

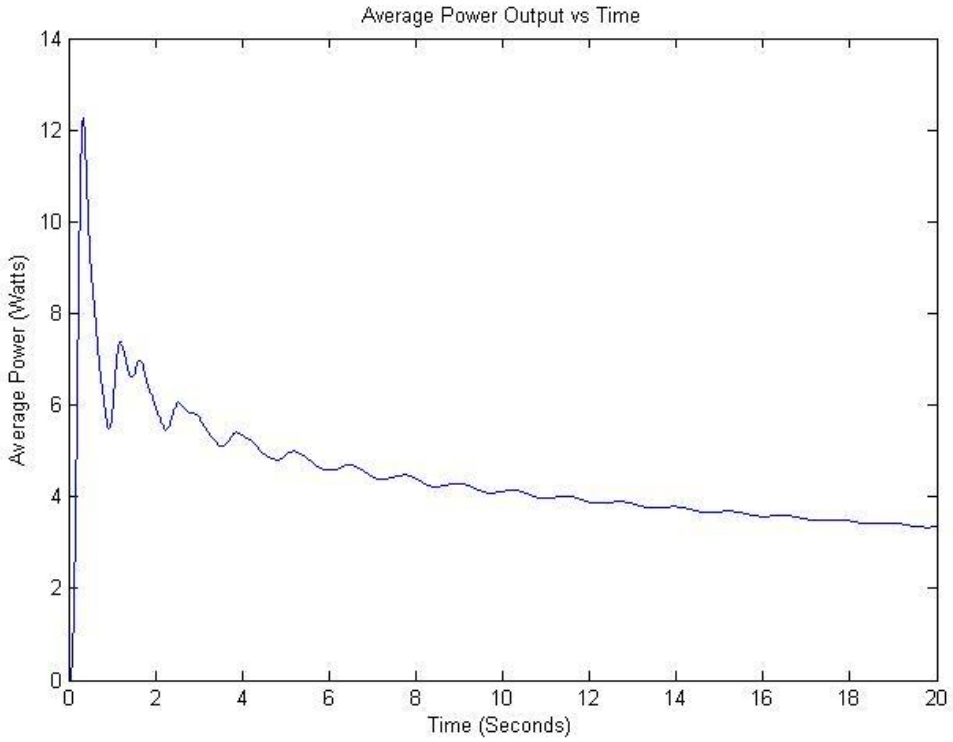

Figure A10: Average power output of the WEC system for a sinusoidal wave input

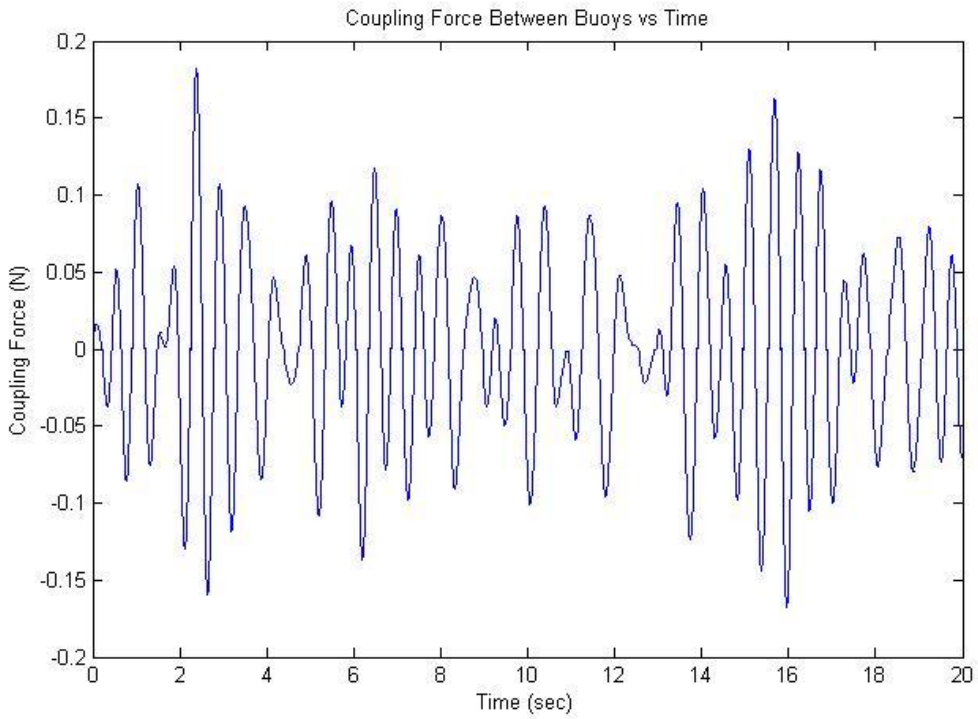

Figure A11: Coupling force of WEC system for a sea state wave input

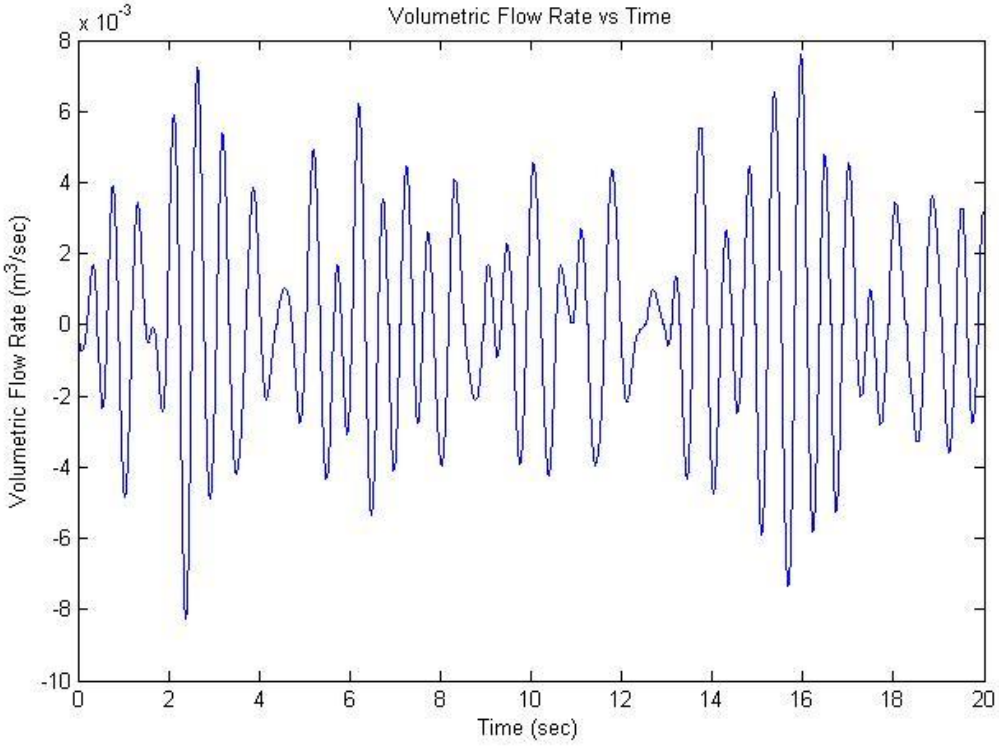

Figure A12: Volumetric flow rate of WEC system for a sea state wave input

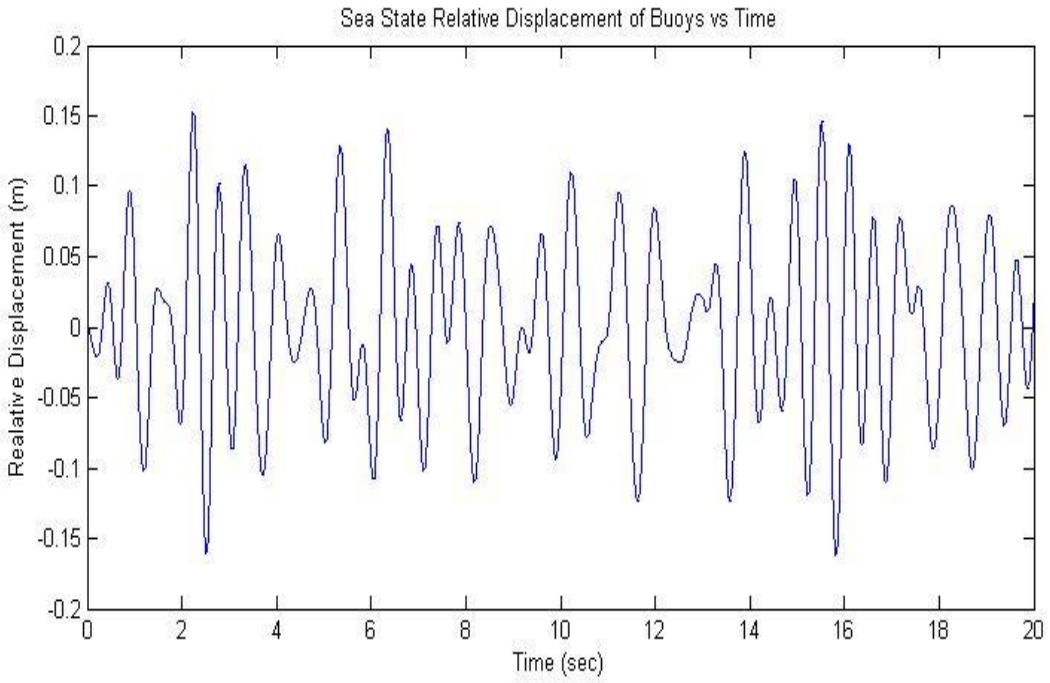

Figure A13: Relative displacement of WEC system for a sea state wave input

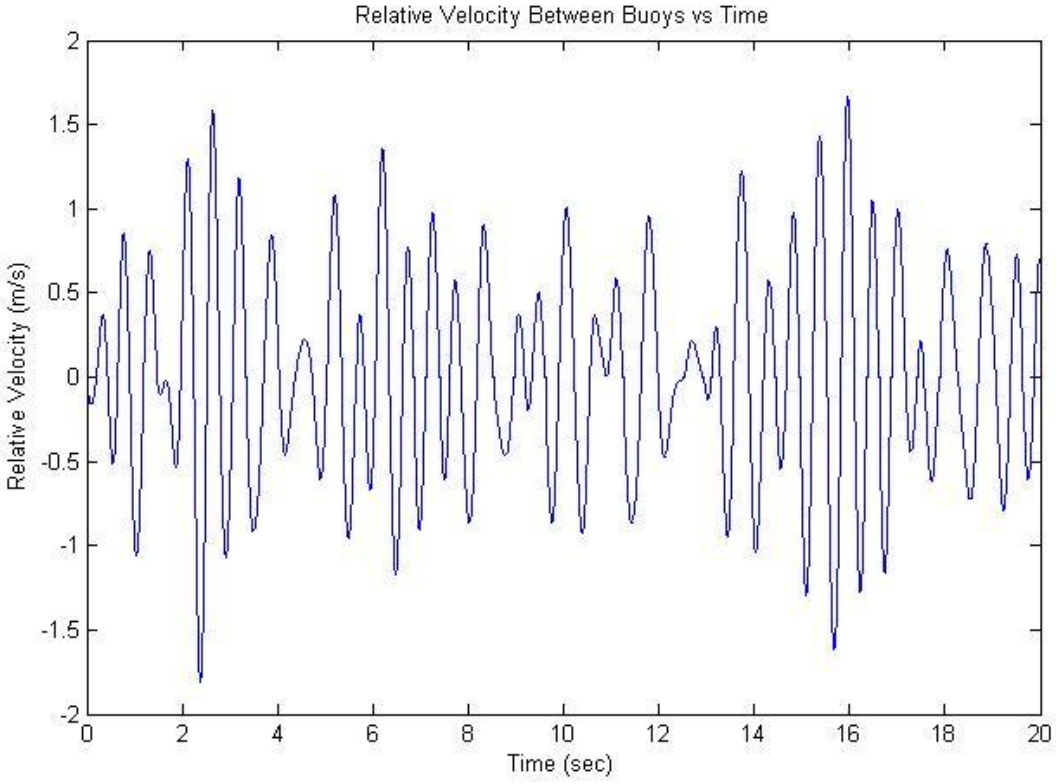

Figure A14: Relative velocity of WEC system for a sea state wave input

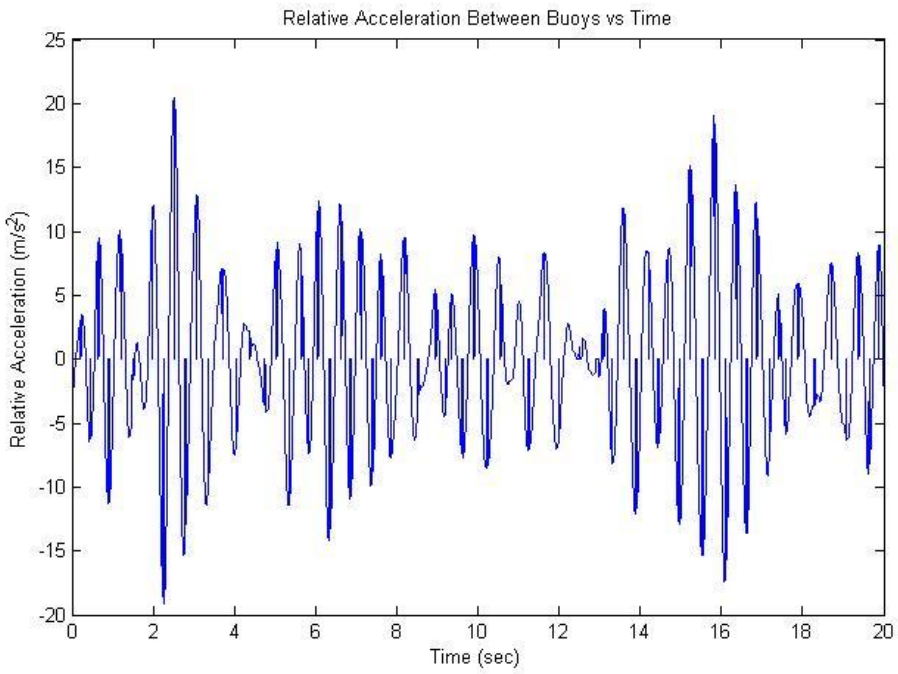

Figure A15: Relative acceleration of WEC system for a sea state wave input

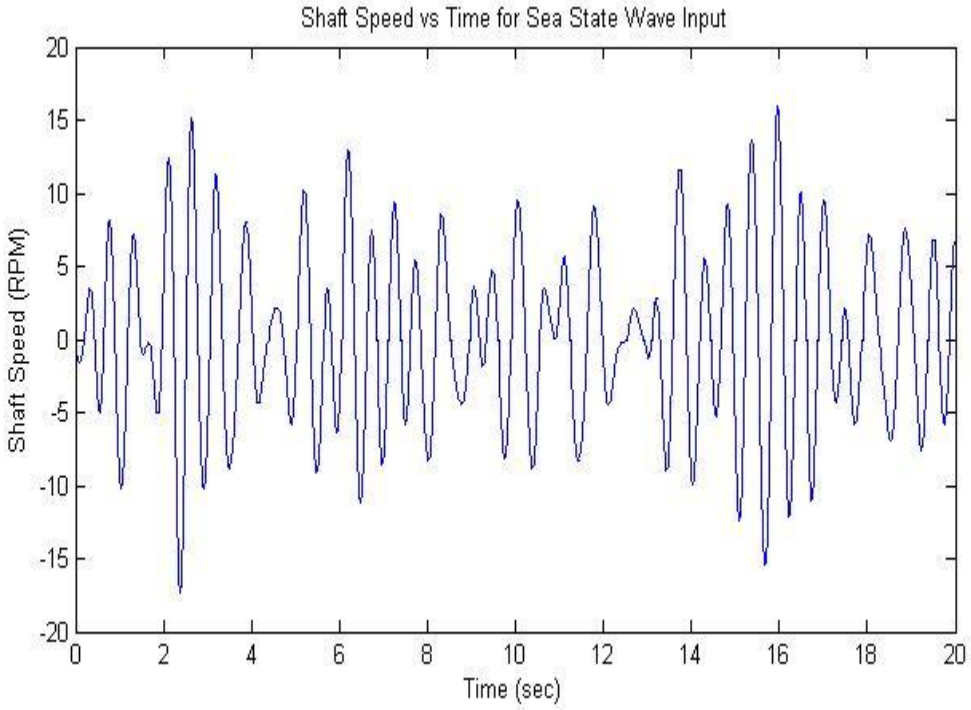

Figure A16: Generator shaft speed of WEC system for a sea state wave input

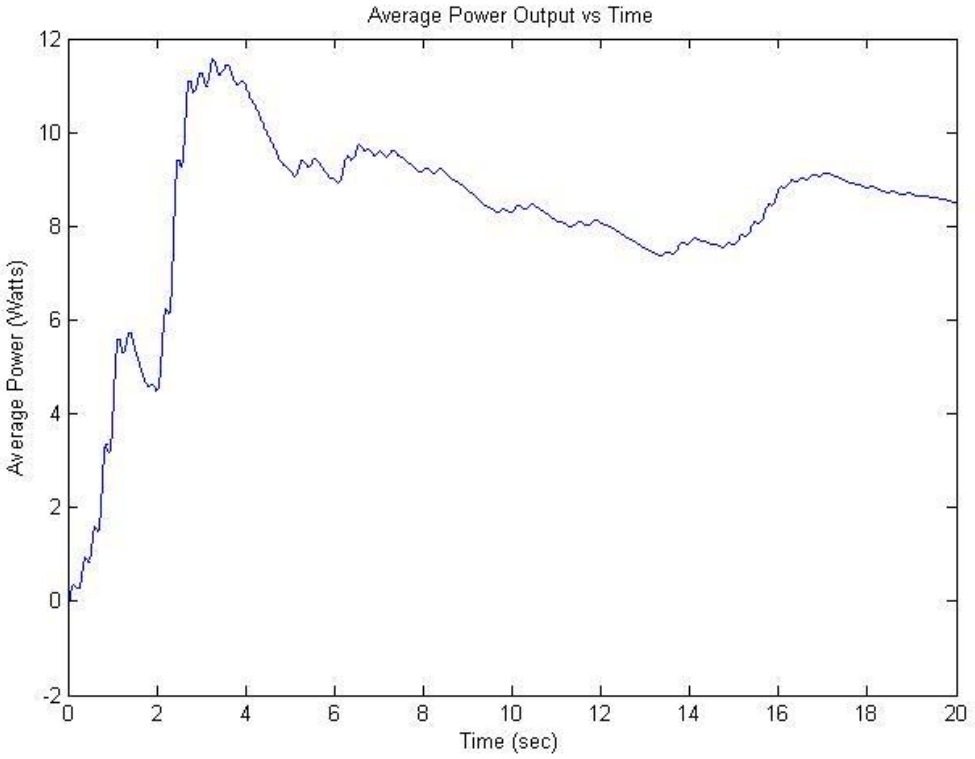

Figure A17: Average power output of WEC system for a sea state wave input

	Reistances Ohms											
Flow Rates (gpm)	3	1.5	1	0.75	0.6	0.5	0.43	0.375	0.33	0.3	0.27	0.25
1	0.86	1.56	2.13	2.61	3.17	3.59	4.07	4.58	5.12	5.46	5.82	6.25
1.2	1.43	2.61	3.57	4.51	5.46	6.41	7.23	7.98	8.96	9.63	10.4 7	11.2 9
1.4	2.10	4.07	5.66	7.24	8.59	10.1 3	11.6 0	13.02	14.4 0	15.7 0	17.1 1	18.3 2
1.5	2.39	4.37	6.25	7.87	9.28	11.0 5	12.4 5	13.98	15.4 8	17.0 3	18.4 0	19.3 6
1.7	2.45	4.58	6.35	8.27	10.0 0	11.4 2	12.7 8	14.35	16.0 3	17.3 3	18.7 3	20.0 7

Table A1: Load data taken from total system testing

Date	Company	Description	Quantity	Price Per Unit	Total Price
1/7/2010	Reimbursement to Megan Kramer	Testing Supplies: see PDF	N/A	N/A	$147.26
1/7/2010	Reimbursement to Aaron Williams	Testing Supplies: see PDF	N/A	N/A	$35.12
1/26/2010	EJP	18" x 13' DR 35 PVC Pipe	13	$23.50	$305.50
		18 RT PVC End Cap	1	$335.00	$335.00
		18 PVC End Plug	1	$180.00	$180.00
3/22/2010	DC Power Supply	Astron 50 Amp Variable DC Regulated Power Supply VS-50M	1	$289.95	$289.95
				Subtotal	**$1,292.83**
				Remaining Budget	$207.17

Table A2: Budget for WEC system